A THEORETICAL APPROACH FOR THE DETERMINATION AND MECHANISTIC INTERPRETATION OF RADIATION D_{10}-VALUE

A Dissertation

by

NONT EKPANYASKUN

Submitted to the Office of Graduate Studies of
Texas A&M University
in partial fulfillment of the requirements for the degree of

DOCTOR OF PHILOSOPHY

May 2009

Major Subject: Biological and Agricultural Engineering

A THEORETICAL APPROACH FOR THE DETERMINATION AND MECHANISTIC INTERPRETATION OF RADIATION D_{10}-VALUE

A Dissertation

by

NONT EKPANYASKUN

Submitted to the Office of Graduate Studies of
Texas A&M University
in partial fulfillment of the requirements for the degree of

DOCTOR OF PHILOSOPHY

Approved by:

Chair of Committee,	Rosana G. Moreira
Committee Members,	M. Elena Castell-Perez
	Leslie A. Braby
	John R. Ford
Head of Department,	Gerald L. Riskowski

May 2009

Major Subject: Biological and Agricultural Engineering

ABSTRACT

A Theoretical Approach for the Determination and

Mechanistic Interpretation of Radiation

D_{10}-value. (May 2009)

Nont Ekpanyaskun, B.S., University of Wisconsin

Chair of Advisory Committee: Dr. Rosana G. Moreira

In the design of the food irradiation process, the knowledge of the radiation resistance of the target organism in a specific food commodity is required. The D_{10}-value, the radiation dose needed to inactivate 90% of the microbial load in the food medium, is used to relate the amount of absorbed energy to the surviving bacterial population. Numerous experimental studies have been performed to determine the D_{10} values of several food-borne microorganisms irradiated under various conditions. Nevertheless, accurate predictions of D_{10} values of the pathogens in food products that have not been empirically examined cannot be made due to insufficient understanding of the biological response to radiation exposure.

A theoretical model for the derivation of the D_{10}-value has been proposed in this study to mechanistically assess the production of radiation-induced DNA damage by energetic electrons. The step-by-step Monte-Carlo simulation technique, which employs the detailed histories of the ionizing particles and the radiolytic species, was utilized. The effects of selected parameters including the genomic sequence, the type of DNA double strand break, the DNA damaging agents, the radical scavengers, the degree of dispersion of DNA molecules, and the number of genome equivalents were hypothetically investigated. The developed computational methodology as well as the results presented can be used as an analytical tool to evaluate the impact of ionizing radiation on cell survival.

DEDICATION

To my family

ACKNOWLEDGEMENTS

I would like to thank my family for their love and support, my advisor and committee members for their guidance and help, the Nuclear Engineering Department, the Laboratory for Molecular Simulation in the Chemistry Department, and the Biological & Agricultural Engineering Department for their cooperation and assistance.

TABLE OF CONTENTS

Page

ABSTRACT iii

DEDICATION iv

ACKNOWLEDGEMENTS v

TABLE OF CONTENTS vi

LIST OF FIGURES viii

LIST OF TABLES ix

CHAPTER

I INTRODUCTION 1

II THEORETICAL BACKGROUND 4

Ionizing radiation in food processing 4
Photon interaction with matter 4
Electron interaction with matter 9
Radiation sources 11
Dose distribution 12
Effect of ionizing radiation on foods and food-borne microorganisms 15
DNA as the target biological molecule 15
DNA repair mechanisms 16
Models for cell survival 20
D_{10}-value 21
Application of Monte Carlo simulation in the assessment of biological damage by radiation 23

III MODEL FORMULATION 25

Simulation of electron transport in water 25
Construction of the target molecules 32
Assessment of DNA damage from direct energy deposition 34
Evaluation of DNA damage by radicals from water radiolysis 35
Determination of D_{10}-value from the resulting DNA damage 42

IV RESULTS AND DISCUSSION 46

D_{10}-value of *E. coli* O157:H7 EDL933 46
Effect of the bacterial genome 47
Effect of n_{bp} and the method of DSB induction 54
Effect of the reaction radii 56
Effect of the scavengers 60
Effect of the detector size 62
Effect of G_{eq} 64
Review of the proposed model and suggestions for improvement 66

CHAPTER Page

V CONCLUSIONS..... 70

REFERENCES 71

VITA 78

LIST OF FIGURES

FIGURE		Page
2.1	Photoelectric process	6
2.2	Compton scattering process	7
2.3	Pair production followed by annihilation of positron	8
2.4	Typical depth-dose curves in a uniform food product irradiated from two sides with gamma rays	13
2.5	Depth-dose curves in a uniform food product irradiated with monoenergetic electron beams at 1, 2, 5, and 10 MeV.....	14
2.6	Survival curve of bacteria exposed to ionizing radiation	22
3.1	Schematic representation of the simulated radiation treatment	31
3.2	Illustrations of DNA molecules inside the detectors	33
3.3	Excitation and ionization cross sections for liquid water.....	38
3.4	Flow chart for the determination of D_{10}-value.....	45
4.1	Survival curves of the cells containing different DNA sequences.....	48
4.2	Average values of electron impact ionization cross sections for the DNA bases	51
4.3	Effect of different values of the reaction radii for the interactions with DNA on the calculated D_{10} values	58
4.4	Changes in the fraction of DSB induced by direct ionization due to the variation of the reaction radii.....	59
4.5	Survival curves of *E. coli* O157:H7 with different G_{eq}	65

LIST OF TABLES

TABLE		Page
3.1	Assumed products of different excitation states	38
3.2	Reaction rate constants for the reactions of the water radicals with the sugar moiety and the nucleobases	40
3.3	Reaction radii for the set of water radiolysis reactions	40
3.4	Diffusion constants for individual species	40
4.1	The percentages of DNA lesion resulting from the direct effect, the damage ratios, and the calculated D_{10} values for the cells with different DNA sequences	48
4.2	95% confidence intervals for the D_{10} values of the cells with similar GC composition	54
4.3	The percentages of DSB due to direct ionization, the damage ratios, and the calculated D_{10} values of *E. coli* O157:H7 for different combinations of n_{bp} and the method of DSB induction	55
4.4	The percentages of DNA damage caused by direct energy deposition and the calculated D_{10} values of *E. coli* O157:H7 for different concentrations of scavengers	61
4.5	The percentages of change in the DNA damage due to the variation in the detector size and the calculated D_{10} values of *E. coli* O157:H7 for different detector volumes	63

CHAPTER I

INTRODUCTION

Food irradiation is a preservation technique that can be used to effectively enhance food safety and prolong the shelf life of food products. The Food and Agriculture Organization of the United Nations (FAO), the International Atomic Energy Agency (IAEA), and the World Health Organization (WHO) conducted a joint study to "review all relevant data related to the toxicological, microbiological, nutritional, radiation chemical and physical aspects" of irradiated foods. The conclusion drawn was that "food irradiated to any dose appropriate to achieve the intended technological objective is both safe to consume and nutritionally adequate" (WHO, 1999). Ionizing radiation has been utilized mainly to eliminate potentially harmful organisms from food materials. However, quality characteristics of certain food commodities can also be improved with irradiation (IAEA, 2002).

Diseases caused by pathogenic microorganisms are of public health concern. Numerous cases linked to the consumption of contaminated food occur on a regular basis. Undoubtedly, radiation technology can help alleviate the magnitude of the problem. Just as with other methods of food preservation, irradiation should be employed with proper manufacturing and handling practices (Parnes & Lichtenstein, 2004; Sommers, 2003). Nevertheless, problems with cross-contamination can be substantially reduced because food items can be packaged before being treated with irradiation (Ahn, Lee & Mendonca, 2006). From the economic viewpoint, food irradiation provides a means to lower financial losses from deterioration of perishable products and expenses due to food-borne illness. Furthermore, this technology can enable food trade that requires fresh produce to be disinfected without significant alteration of the physical properties.

The association of the term ionizing radiation to the hazardous radioactive materials creates a strong barrier to public acceptance. One must realize that the radiant energy is only present during the exposure. These forms of high-energy radiation disappear after the treatment.

This dissertation follows the style of *Food Chemistry*.

Any concern regarding the formation of radiolytic species, mutation, or loss of nutrients as a result of the use of ionizing radiation should be discussed by comparison with other conventional methods such as thermal or high pressure processing. Normally, to attain the same level of pasteurization, radiation induces similar types of chemical and biological changes incurred by other decontamination techniques but to a lesser extent (Crawford & Ruff, 1996; Parnes & Lichtenstein 2004; Shea and the Committee on Environmental Health, 2000). Misconceptions should be addressed in a scientific manner to prevent unjustified concerns over the safety of irradiated foods.

To improve the efficiency of any process, the underlying principles must be understood. For the design of a specific irradiation treatment, the dose response of the target organism must be predetermined. D_{10}-value, the dose required to inactivate 90% of the microbial population, is employed as a measure of the radiation resistance of a microorganism. Several experiments have been conducted to determine the D_{10}-values of various microbes in diverse food materials. Speculations of the factors influencing the D_{10} values have been made from the published experimental data. However, current knowledge of irradiation technology is insufficient for accurate prediction of the radiation response of a particular microorganism subjected to an unprecedented experimental condition to be achieved. Comprehension of how and the extent to which each relevant variable mechanistically affects the microorganism's ability to tolerate the radiation insult has not been adequately established.

The objective of this research was to develop a computational methodology to determine the D_{10} values using existing mathematical models and data from the literature. The theoretical model formulated allows assessment of different aspects of the induction of molecular damage. Both direct and indirect effects of radiation on the microbial DNA were systematically investigated by means of step-by-step Monte-Carlo simulation. The impact of selected factors presumed to be influential on the radiation sensitivity was hypothetically examined. The implications of the research findings for food processing were discussed. The reliability of the proposed algorithm was reviewed. Future directions for model improvement were also suggested. The developed

algorithm presented in this study can be used as an investigative tool in concert with other methods to provide greater insight into the lethal effect of radiation on cell survival.

CHAPTER II

THEORETICAL BACKGROUND

Ionizing radiation in food processing

In food irradiation, gamma (γ) rays, X-rays, and electron beams are the three types of radiation used to eliminate potential hazards from food-borne organisms. Gamma rays and X-rays are electromagnetic radiations called photons. They both possess the same physical properties at any given quantum energy. The difference between the two is their modes of origin. Gamma rays are emitted from nuclei or in annihilation reactions between matter and antimatter whereas X-rays are emitted by charged particles in changing atomic energy levels or in slowing down in a Coulomb force field. Unlike gamma rays and X-rays, electrons are charged particles. They can be emitted from nuclei or result from charged particle collisions (Attix, 1986).

The interaction of ionizing radiation with matter is stochastic in nature. As the incoming particle comes close enough to interact with an atom, there is more than one possibility of what could happen. The interaction might be elastic, in which the particle is deviated from its path without any loss of its energy, or inelastic, by means of which the energy loss from the incoming particle results in ionization or excitation of the molecule (Uehara, Nikjoo & Goodhead, 1999). Each type of interaction is associated with different probabilities which depend on the characteristics of the ionizing particle and the matter being traversed.

Photon interaction with matter

Because photons are electrically neutral, they can travel freely through empty space without steadily losing energy until interacting with an atom in the attenuating material (Turner, 2007). At the point of interaction, a photon can undergo one of the competing processes. The main modes of photon interaction are photoelectric effect, Compton scattering, and pair production. Other types of interactions, i.e., Rayleigh scattering (elastic scattering of a photon by the action of the whole atom) and photodisintegration (disintegration of a nucleus by high-energy

photon penetration), are not important in the food irradiation process. The regions of dominance of different modes depend on the atomic number (Z) of the absorber and the photon energy (Attix, 1986). For instance, Compton scattering dominates much of the energy range for low-Z materials; whereas a low-energy photon is very likely to experience the photoelectric effect when traversing a high-Z material.

Photoelectric effect

In the photoelectric process, an incident photon interacts with an orbital electron causing the bound electron to be ejected from the scattering atom. The photon transfers all of its energy to the photoelectron. For this process to take place, the energy of the incident photon, $h\nu$, must be equal to or greater than the binding energy of the electron, E_b , in the respective orbital. The energy of the photoelectron, $E_{photo\ e^-}$, is

$$E_{photo\ e^-} = h\nu - E_b \,. \tag{2.1}$$

The ejection of the inner-shell photoelectron leaves the shell vacant during the time in which the atom is excited. An outer-shell electron with a lower binding energy then moves to fill the vacancy. This step is followed by the emission of the fluorescence (characteristic) X-ray with the energy equal to the difference in the binding energies of the two orbital electrons. An alternative mechanism of losing energy is the non-optical transition known as the Auger process. Instead of emitting fluorescence X-rays, the atom can opt to eject one or more outer-shell electrons called Auger electrons to get rid of the excess energy (Attix, 1986). The illustration of the photoelectric absorption process is given in Figure 2.1.

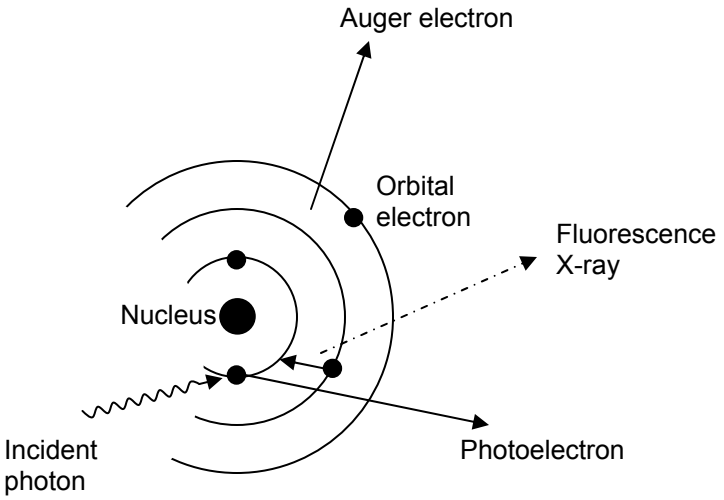

Figure 2.1. Photoelectric process (adapted from Alpen, 1998)

Compton scattering

The Compton scattering process is the phenomenon in which an incident photon with an energy $h\nu$ transfers some of its energy to a loosely bound or unbound electron at their encounter (see Figure 2.2). The scattered photon leaves the site of interaction with the lower energy $h\nu'$ at the scattering angle θ from its original direction. The recoil electron with the kinetic energy E_{Comp} departs at the angle ϕ relative to the incident photon's track. The relationships between the energies and the directions of the interacting photon and electron are given below (Alpen, 1998; Attix, 1986):

$$E_{Comp} = h\nu - h\nu' \tag{2.2}$$

$$h\nu' = \frac{h\nu}{1 + \left(\frac{h\nu}{m_0 c^2}\right)(1 - \cos\theta)} \tag{2.3}$$

$$\cot\phi = \left(1 + \frac{h\nu}{m_0 c^2}\right)\tan\left(\frac{\theta}{2}\right) \tag{2.4}$$

where $m_0 c^2$ is the rest energy of the electron.

For an incoming photon with low energy, the energy transfer will be small and the scattered photon will retain most of its energy after the interaction. When no energy is transferred during the deflection of the photon, the process becomes Thomson scattering where both the incident and scattered photons possess the same frequency. As the energy of the incoming photon increases, the free electron could receive a greater portion of the incident photon energy. However, the photon cannot transfer all of its energy to a free electron through Compton scattering process, e.g., for a very high-energy incident photon, the energy of the corresponding 180^{o} backscattered photon will approach 0.2555 MeV (Attix, 1986).

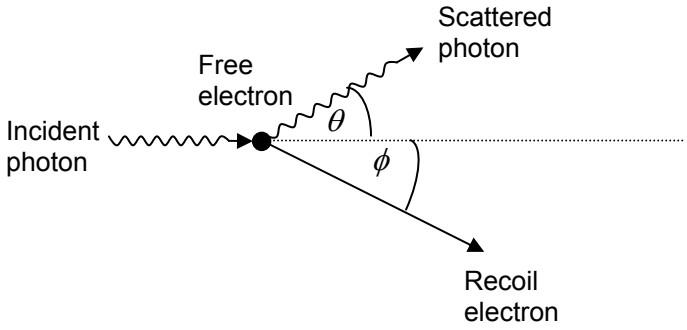

Figure 2.2. Compton scattering process (adapted from Alpen, 1998)

Pair production

When a photon having energy greater than twice the electron rest energy, $2m_0c^2$ or 1.022 MeV, travels near the nucleus of an atom, the photon could experience the strong field effects and disappear in the energy to mass conversion giving rise to a pair of an electron and a positron. The total kinetic energy of the electron (E_{e^-}) and positron (E_{e^+}) is

$$E_{e^-} + E_{e^+} = h\nu - 2m_0c^2 . \qquad (2.5)$$

The amount of excess energy can be allocated in any proportion between the generated electron and positron. The newly formed electron and positron traverse the medium and lose their energy via excitation and ionization of atoms. The annihilation reaction occurs when the positron approaches the rest energy and reacts with another free electron. Two photons, each of 0.511

MeV, emerge from the conversion of mass to energy and leave the production site in the opposite direction as the positron and the encountered electron annihilate (Alpen, 1998). The processes of pair production and annihilation of the positron are shown in Figure 2.3.

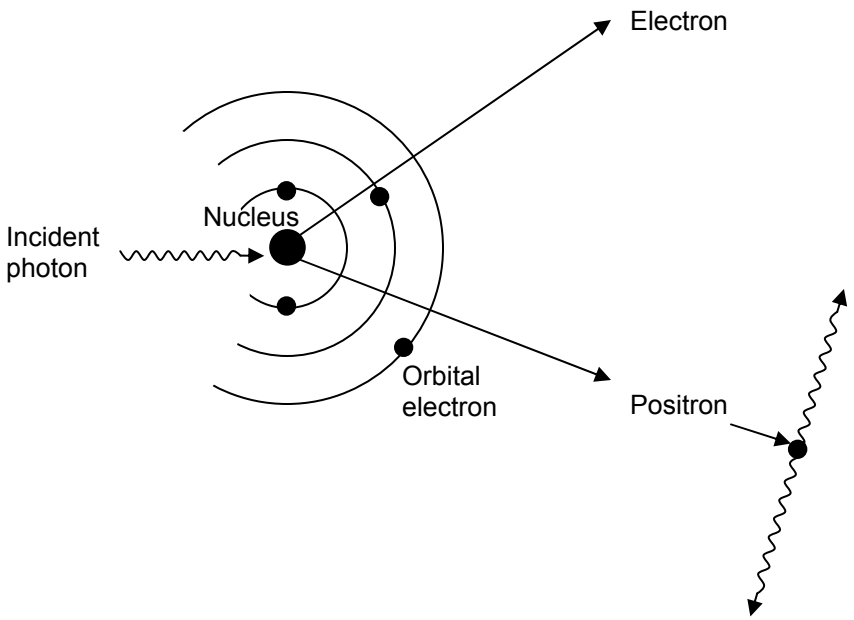

Figure 2.3. Pair production followed by annihilation of positron (adapted from Alpen, 1998)

Attenuation, energy-transfer, and energy-absorption coefficients

If monoenergetic photons traverse a uniform medium in the x-direction, the number of uncollided photons will decrease exponentially as a function of distance (Turner, 2007):

$$N_{pho}(x) = N_{pho_0} e^{-\mu x} \tag{2.6}$$

where $N_{pho}(x)$ is the number of photons that have not interacted at depth x, $N_{pho_0}(x)$ is the number of initial photons at x = 0, and μ is the linear attenuation coefficient.

The constant μ is the sum of the linear attenuation coefficients for the individual physical processes. The mass attenuation coefficient is μ divided by the density, ρ. The total mass energy-transfer coefficient, $\frac{\mu_{tr}}{\rho}$, can be calculated as:

$$\frac{\mu_{tr}}{\rho} = \frac{\tau_{tr}}{\rho} + \frac{\sigma_{c\,tr}}{\rho} + \frac{\kappa_{tr}}{\rho} \tag{2.7}$$

where $\frac{\tau_{tr}}{\rho}$, $\frac{\sigma_{c\,tr}}{\rho}$, and $\frac{\kappa_{tr}}{\rho}$ are the mass energy-transfer coefficients for the photoelectric effect, Compton scattering, and pair production respectively.

The equation above can be rewritten for photons of energy $h\nu$ with the linear attenuation coefficients for photoelectric effect (τ), Compton scattering (σ_c), and pair production (κ) as:

$$\frac{\mu_{tr}}{\rho} = \frac{\tau}{\rho}\left(1 - \frac{\delta}{h\nu}\right) + \frac{\sigma_c}{\rho}\left(\frac{T_{c\,avg}}{h\nu}\right) + \frac{\kappa}{\rho}\left(1 - \frac{2mc^2}{h\nu}\right) \tag{2.8}$$

where δ is the average energy of the fluorescence emission following the photoelectric absorption and $T_{c\,avg}$ is the average kinetic energy of the Compton electron.

The mass energy-absorption coefficient, $\frac{\mu_{en}}{\rho}$, can be determined as:

$$\frac{\mu_{en}}{\rho} = \frac{\mu_{tr}}{\rho}(1 - g) \tag{2.9}$$

where g is the fraction of the initial kinetic energy transferred to electrons that is further emitted as bremsstrahlung.

The experimental values of these coefficients for different absorbers are widely available in the literature (Turner, 2007).

Electron interaction with matter

Electrons, like other charged particles, are surrounded by Coulomb electric force field. Hence, they lose kinetic energy gradually through Coulomb-force interactions with the atoms of the traversed matter. A series of deflections from interactions before an electron comes to rest yields a tortuous electron path in the medium. The charged-particle Coulomb-force interactions can be characterized into three types: soft collision, hard collision, and the interaction with the external nuclear field (Attix, 1986).

Soft collision occurs when a charged particle passes an atom at a large distance, i.e., the separation between the traversing particle and the nucleus of the atom is considerably greater than the atomic radius. The particle's Coulomb force field can affect the atom by exciting it to a higher energy state or ionizing it by dislodging a valence electron. This type of interaction is the most probable. However, the energy transfer per interaction is small when compared to that of the hard collision.

Hard or knock-on collision takes place when a charged particle encounters an atom at a distance approximately equivalent to the atomic radius from the nucleus. A single atomic electron is likely to be ejected after the collision. The knock-on electron (secondary electron or delta ray) will also experience Coulomb-force interactions on a separate track. If the inner-shell electron is knocked off, the outer-shell electron will move to fill the vacancy followed by the process of emitting fluorescence and/or Auger electron. Since both the primary and secondary electrons have the same physical properties, by convention, the one that has a higher energy between the two is considered to be the primary electron.

If a charged particle travels very close to the nucleus, i.e., the distance from the charged particle to the nucleus is much smaller than the atomic radius, such particle could undergo the Coulomb-force interaction with the external nuclear field. An electron can interact with the nucleus either elastically or inelastically. In most cases, the electron will be scattered without losing a significant amount of energy to the nucleus. However, in about 2-3% of the time, the electron can lose up to 100% of its kinetic energy through radiative interaction. Consequently, the electron is deflected and slowed down while bremsstrahlung is emitted in the process.

The average rate of energy loss per unit path length of charged particles in matter can be quantified by the stopping power or linear energy transfer (LET). The stopping power is specific for the type of charged particle, kinetic energy, and atomic number of the attenuating medium. The total stopping power for electrons is the sum of the collision and radiative stopping powers (Attix, 1986).

Radiation sources

The radioisotopes permitted to be used as the sources of gamma rays in food processing are Cobalt-60 and Cesium-137. X-rays and electron beams can be generated from machines powered by electricity. The maximum energies for X-rays and electron beams to be utilized in accordance with Codex Alimentarius are 5 and 10 MeV respectively. The energy limits were set to prevent the possibility of inducing radioactivity in the irradiated food via photonuclear reactions (IAEA, 2002).

Depending on the nature of the products, one form of radiation is more suitable than another. For the product that is relatively thin (smaller than twice the penetration depth of the electrons) and can be radiated at a high dose rate, electron beam is a more appropriate choice. However, for thicker products, gamma rays or X-rays must be employed due to their greater penetrating capability (IAEA, 2002). Nevertheless, the design of the irradiation process must take into account the operating cost and the production level in order to make the process economically viable.

Gamma ray emitters

Cobalt-60 is unstable with a half-life of 5.3 years, i.e., its radioactivity will be reduced to half after a period of 5.3 years. This radionuclide disintegrates into a stable isotope of nickel:

$$^{60}_{27}Co \rightarrow ^{60}_{28}Ni + \ ^{0}_{-1}e + \ ^{0}_{0}\bar{\nu} + \gamma \, . \tag{2.10}$$

Two photons (γ) of energies 1.17 and 1.33 MeV as well as an electron, $^{0}_{-1}e$, and an anti-neutrino, $^{0}_{0}\bar{\nu}$, are emitted from the beta-minus decay process.

Cesium-137 has a half-life of 30.0 years. It beta decays to Barium-137. The resulting photon has the energy of 0.66 MeV.

$$^{137}_{55}Cs \rightarrow ^{137}_{56}Ba + \ ^{0}_{-1}e + \ ^{0}_{0}\bar{\nu} + \gamma \tag{2.11}$$

Note that 5% of the time, the beta particles carry out all the energy and no photon is emitted.

Since these radioisotopes always disintegrate, gamma rays are emitted even when they are not in use. Replenishment of the radionuclide source must be performed periodically in order to maintain the same level of throughput capacity (Wilkinson & Gould, 1996).

Electron beam and X-ray machines

Electron beams and X-rays can be produced by electron accelerators. Two basic types of accelerators commonly used are the steady current type, e.g., the Van de Graaff accelerator, and the pulsed beam type, e.g., the linear accelerator (LINAC). The bremsstrahlung X-rays can be generated by distributing the electron beam over a high-Z target such as tungsten or tantalum. The resulting X-rays will have a broad energy spectrum unlike the gamma rays emitted from Cobalt-60 or Cesium-137 (IAEA, 2002). The advantage of using electron beams or X-rays is that the potential hazard from handling the radioactive materials is eliminated.

Dose distribution

The quantity that is used to describe the amount of energy absorbed in the medium is called dose. It is defined as the energy deposited by ionizing radiation per unit mass. The SI unit of dose is the gray (Gy) which is equivalent to 1 joule of radiant energy per kilogram of irradiated material. Accordingly, the dose rate is the dose per unit time.

The amount of absorbed dose is not exactly the same from one point to another in the irradiated food product. Low dose uniformity ratio, the ratio between the maximum and the minimum absorbed dose at any depth, is often desired in the irradiation treatment. Shown in Figure 2.4 is the illustration of the dose distribution in a gamma irradiated food sample. The object is irradiated from two sides, left and right. The doses received from exposure on the left and right are designated by D_l and D_r respectively. The dose $D_l + D_r$ is the absorbed dose in the sample as a result of two sided irradiation. The shape of the depth-dose curve comes from the exponential attenuation characteristic of monoenergetic photons (IAEA, 2002).

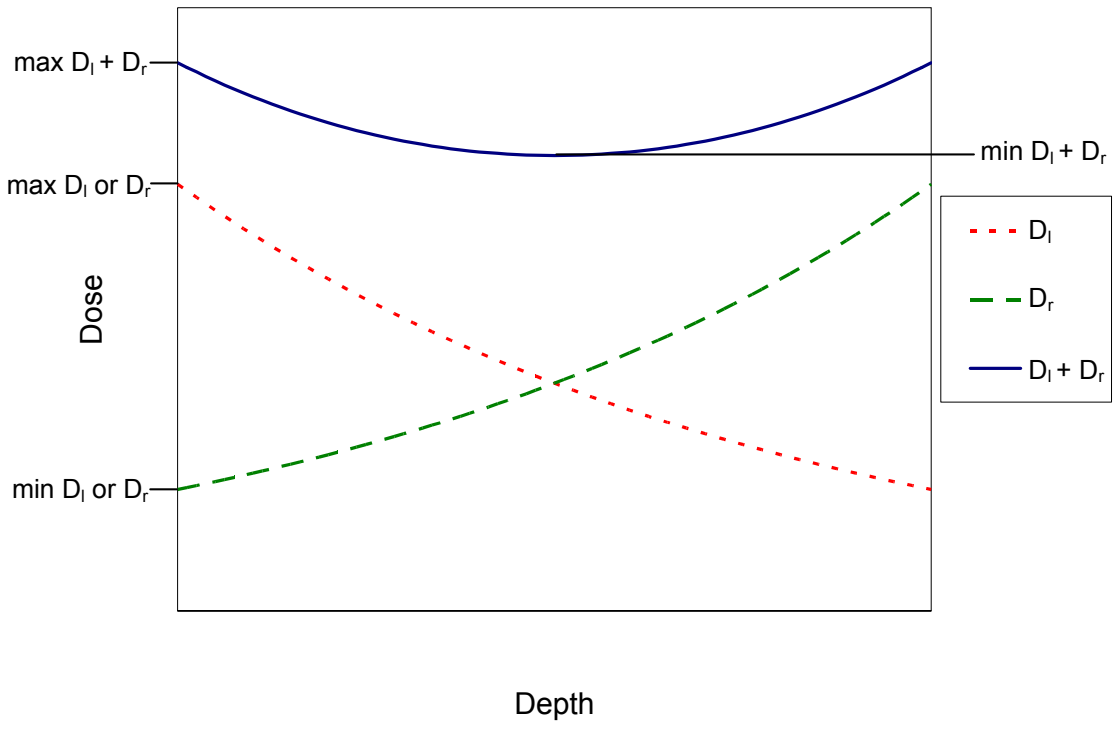

Figure 2.4. Typical depth-dose curves in a uniform food product irradiated from two sides with gamma rays (adapted from IAEA, 2002)

The depth-dose distribution in a uniform food sample irradiated by electron beams at various energies is demonstrated in Figure 2.5. The maximum absorbed dose is not at the surface but at a distance inside the irradiated product due to the scattering effect and the contribution of energy deposition by secondary electrons. The higher the electron energy the greater the penetration depth; however, the ratio between the maximum absorbed dose and the dose at the surface becomes smaller as the initial energy of the electrons increases. Two sided irradiation by electron beams can also give the product a better uniformity of the dose distribution just like in the case of gamma irradiation.

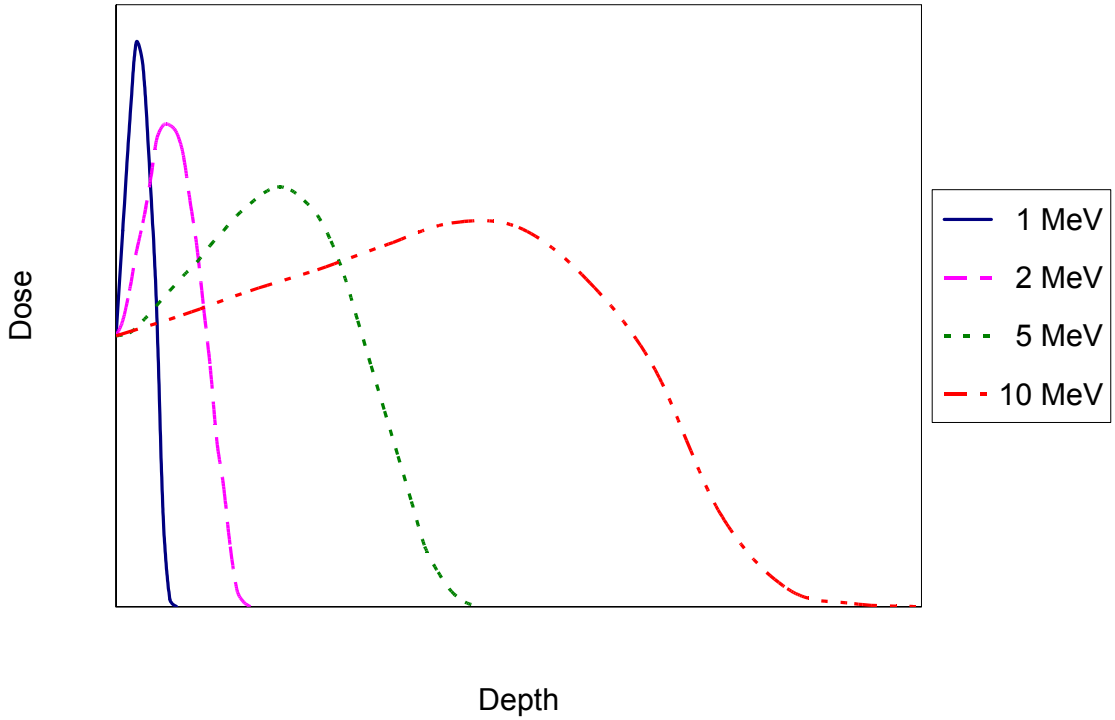

Figure 2.5. Depth-dose curves in a uniform food product irradiated with monoenergetic electron beams at 1, 2, 5, and 10 MeV (adapted from Tabata, Andreo & Ito, 1991)

The dose distribution can be obtained empirically by the dose-mapping technique. In this technique, the dosimeters are placed throughout the host material prior to radiation processing. The dose readings from dosimeters associated with different positions in the irradiated sample are employed to construct the dose map after the treatment. The material used as a dosimeter must have a well characterized radiation response for the operating dose range and must behave similarly to the food sample in terms of radiation interactions (IAEA, 2002). Other methods such as Monte Carlo simulation have also been utilized to calculate the dose distribution inside the food products (Kim, Moreira, Huang & Castell-Perez, 2007; Kim, Moreira, Rivadeneira & Castell-Perez, 2006; Kim, Rivadeneira, Castell-Perez & Moreira, 2006). Nevertheless, a number of sources of error such as the inaccuracy of the calibration and the assumptions made in the method always lead to uncertainty in dose determination.

Effect of ionizing radiation on foods and food-borne microorganisms

Foods are composed of carbohydrates, proteins, lipids, vitamins, and other nutrients. These components are chemical compounds, which consist of elements chemically bonded together. The cell of the microorganism also contains sets of compounds. Hence, the immediate effects of radiation on food and its components as well as the food-borne microorganism, i.e., the initial results of photon or electron interactions with particular atoms, can be described by different types of interactions elucidated above. However, the subsequent effects of irradiation on the functionality of each compound vary.

When molecules receive radiant energy above their ionization thresholds, they can be ionized, creating positive and negative ions. As a result, free radicals, the species that have at least one unpaired electron, are formed and interact with each other and the nearby molecules. The species that absorbs energy but does not lose its orbital electron is excited. The excited molecules or compounds can lose their energies through a variety of dissociation schemes generating more free radicals of different kinds. These radicals are reactive. A series of complex chemical reactions takes place until the stable final products are formed.

For living organisms, biological changes can be attributed to the direct and indirect actions of radiation. The direct effect is caused by the deposition of radiation energy in the target biological molecule whereas the indirect effect is the result of the attack of the radiolytic radical previously produced by the absorbed radiant energy. The degree to which the radiolytic radicals are responsible for the damage depends on the number of reactions with the target molecules. Any technique that can prevent the reaction from occurring such as immobilizing the radicals by freezing the food material can reduce the indirect effect of irradiation.

DNA as the target biological molecule

Deoxyribonucleic acid (DNA) is a polymer of nucleotides. A molecule of DNA consists of sugar-phosphate backbones and nitrogenous bases. The type of sugar in the backbone is 2'-deoxyribose. Four nitrogenous bases in DNA are adenine (A), cytosine (C), guanine (G), and thymine (T). The purine bases, A and G, always pair with the pyrimidine bases, T and C,

respectively. DNA stores genetic information through the sequence of the bases. Each polynucleotide chain of the double-helical DNA is complementary to its counterpart and can be used as a template for DNA replication. Geometrically, the hydrophilic sugar-phosphate backbones are on the outside whereas the hydrophobic nitrogenous bases are on the inside of the DNA double helix. The B-form DNA, which is the most stable structure, has a right handed helical sense. Its diameter is approximately 20 Å. The number of base pairs per helical turn is 10.5 and the base pairs are stacked 3.4 Å apart. A and Z forms of DNA have also been proposed but the B-form is regarded as the standard form of DNA (Nelson & Cox, 2005).

DNA is known to be the most important target of ionizing radiation. Other macromolecules can lose their biological activities as a consequence of radiation damage. However, many of them can be quickly synthesized and replaced. Any alteration or destruction of the DNA molecule, which contains genetic information necessary for self-replication, biochemical renewal, and cell division, can cause the cell to lose its ability to survive or reproduce. Different types of DNA lesions include double and single strand breaks of the duplex molecules, chemical alteration of the bases and the sugar moieties, and cross linking to related matrix proteins and nucleotides. When at least one complementary strand still remains intact, the repair process can be carried out with high fidelity. A double strand break, DSB, on the other hand, is likely to cause a loss of some genetic information. Hence, DSB is the most crucial DNA lesion that determines the fate of the cell (Alpen, 1998).

DNA repair mechanisms

There are several possibilities that the repair systems in the cell can accommodate the damages in the DNA. Some of these enzyme systems can repair a range of DNA lesions while others can handle only a specific type of damage. A well-known radioresistant bacterium *Deinococcus radiodurans* has the enhanced DNA repair capacity in comparison to most microorganisms; and the loss of this capacity makes *D. radiodurans* more vulnerable to ionizing radiation (Zimmermann & Battista, 2006). The ability of any organism to cope with the radiation insult depends largely on its innate DNA repair systems. The major repair pathways are given

below. In addition, the mechanisms of repair processes in *Escherichia coli*, the most studied organism in biology, which is also the microbe of interest in food irradiation, are provided.

Nucleotide excision repair

Nucleotide excision repair (NER) is a highly versatile pathway which can remove a variety of helix-distorting DNA lesions. NER pathway can be divided into five general steps: damage recognition, incision of the damaged strand, excision of the lesion-containing oligonucleotide, new DNA synthesis, and ligation.

NER in *E. coli* begins with the dimerization of two UvrA molecules, followed by the formation of a heterotrimer with one molecule of UvrB. The UvrA-UvrB complex binds to the DNA and translocates along the DNA strand. When the distorting lesion is encountered, UvrB forms the UvrB-DNA complex at the damage site inducing a specific DNA conformation. At that point, two UvrA proteins are released from the DNA. Another protein, UvrC, then binds to the UvrB-DNA complex and makes two incisions in the damaged strand. The oligomer containing the lesion (a fragment of 12 to 13 nucleotides) as well as UvrC are released as the UvrD helicase attaches to the DNA and unwinds the DNA helix. The incorporation of the new nucleotides to the gap is accomplished by DNA polymerase I during the dissociation of UvrB. The nicks are sealed by DNA ligase at the end of the repair process (Hoeijmakers, 1993).

Base excision repair

The base excision repair (BER) pathway can be used to repair the damaged or modified DNA bases, sites of base loss, single strand breaks, and short gaps in DNA. The altered DNA bases are recognized and removed by DNA *N*-glycosylases. The enzyme cleaves the *N*-glycosylic bond between the unwanted base and the sugar moiety to produce an abasic (apurinic or apyrimidinic) site. The incision of the sugar-phosphate backbone at the abasic site is performed by an AP endonuclease.

Two major types of AP endonuclease in *E. coli* are AP lyase (class I) and true AP endonuclease (class II). The class I AP endonuclease or AP lyase catalyzes the incision of the

phosphodiester linkage at the 3'-side of the abasic site by β-elimination. This cleavage leaves a 5'-phosphate group and a 3'-terminus that requires removal by a class II AP endonuclease/3'-diesterase. The class II AP endonuclease, however, incises the 5'-side of an abasic site, generating a 3'-OH terminus and a 5'-abasic residue left to be removed by a deoxyribophosphodiesterase.

After the nonconventional DNA terminus created by either class I or II AP endonucleases is removed, the single-base gap formed is then filled by DNA polymerase I. Finally, DNA ligase seals the single-strand nick to complete the BER pathway. Note that in *E. coli*, class II AP endonucleases constitute more than 90% of the total cellular AP endonuclease activity (Kow, 1994; Wilson III, Engelward & Samson, 1998).

Mismatch repair

Mismatch repair is the mechanism that recognizes the mispaired bases and replaces them with the correct ones. Some systems in *E. coli* such as very-short-patch repair can process only specific mismatches. However, the DNA adenine methyltransferase (Dam) directed DNA mismatch repair, abbreviated as DDMR, can repair all possible base mispairs with only one exception, the C·C mismatch.

In DDMR, the methylated adenine in the sequence d(GATC) is used to distinguish between the intact template and the incorrect strand. The MutS protein first detects and binds to the mismatch. MutL then forms a complex with MutS and MutH proteins to facilitate bending of the DNA into a looped structure. The MutH endonuclease cleaves the strand that contains the mispaired base at the GATC site closest to the mismatch. The DNA is separated by the UvrD helicase. Depending on the location of the nick, the bases are removed by either ExoI, ExoVII, or RecJ. The excision tract, which can be thousands of base pair in length, is filled by DNA polymerase III and the nicks are sealed by DNA ligase (Rasmussen, Samson & Marinus, 1998).

Homologous recombination

Homologous recombination is a mechanism that utilizes the information on the homologous, intact chromosome to repair a DSB on the damaged chromosome. In *E. coli*, RecBCD enzyme recognizes the DSB and binds to the free ends of DNA. The enzyme unwinds the duplex as it moves along the DNA. At first, both strands of the DNA are degraded by the dual 5'→3' and 3'→5' exonuclease activities of RecBCD. Once RecBCD encounters a specific DNA sequence: 5' GCTGGTGG 3' called Chi, its 3'→5' exonuclease activity is inhibited while its 5'→3' activity is enhanced generating a recombinogenic end.

This single stranded 3'-hydroxyl end is then coated with multiple RecA proteins. RecA protein catalyzes strand invasion, homologous pairing, and formation of Holliday-type structure then leaves the site. RuvA protein recognizes and binds to the center of the Holliday junction. Two hexameric RuvB proteins form the complex with RuvA protein and promote branch migration. RuvC endonuclease proteins then bind to the RuvA-RuvB complex and cleave the DNA intermediate. Subsequent ligation of the cut ends completes the recombination process (Lodish, Berk, Zipursky, Matsudaira, Baltimore & Darnell, 2000).

Direct reversal

Some types of DNA modification can be repaired without any breakage of the sugar-phosphate backbone. No nucleotide or nitrogenous base is removed and replaced during the repair process. An example of direct reversal of DNA damage is the repair of cyclobutane pyrimidine dimer, Pyr<>Pyr , by the photoreactivating enzyme DNA photolyase.

The *E. coli* DNA photolyase is a monomeric polypeptide of 471 amino acids containing two cofactors, flavin adenine dinucleotide and methenyltetrahydrofolate. In the photoreaction, the DNA photolyase recognizes and attaches to the Pyr<>Pyr regardless of the light condition. When exposed to a photon of appropriate wavelength, the photon energy is first absorbed by methenyltetrahydrofolate then transferred to the reduced flavin adenine dinucleotide via dipole-dipole interaction. An electron is donated from the activated intermediate to the Pyr<>Pyr. As a result, the 5-5 and 6-6 bonds of the cyclobutane ring are split generating a Pyr and a Pyr^{-}.

An electron from Pyr^- is transferred back to the flavin cofactor to return the enzyme to its original state. The enzyme dissociates from the DNA and the two pyrimidines are restored (Rupp, 1996; Sancar, 1994).

Models for cell survival

The cell survival curve has been extensively used in radiation biology to provide the relationship between the fractional survival of a population of radiated cells and the radiation dose administered. The survival probability at each dose level represents the fraction of the cells that still have the ability to reproduce after being treated with radiation. Note that the reproductive death is not equivalent to the complete cessation of cell activities. The dose required for clonogenic death is much lower than that necessary to completely suppress the metabolic and respiratory activities of a cell (Alpen, 1998).

Many mathematical models have been proposed to describe the principles behind the survival curves. Lea's target theory is one of the earliest models for cell killing. The theory proposes that when radiation energy is deposited in the sensitive volume(s) or target(s), the cell will not survive. For the simplest case, in which there is one target in the cell and only one hit is sufficient for total inactivation, the number of viable organisms N that survive the dose D^* can be determined as (Lea, 1955):

$$N = N_0 e^{-\frac{D^*}{D_0}} \tag{2.12}$$

where N_0 is the initial number of organisms and D_0, also known as D_{37}, is the dose needed to score an average of one hit per organism.

Target theory has been widely accepted to explain the actions of ionizing radiation on microorganisms of which the survival curves are exponential. For the cells of higher organisms such as mammals, the survival curves exhibit a sigmoidal shape which has been attributed to the more complex DNA repair system.

Mathematical formalisms such as the linear-quadratic model of Chadwick and Leenhouts (1973), the dual radiation action model of Kellerer and Rossi (1978), the repair-misrepair model of

Tobias (1985), and the lethal-potentially lethal model of Curtis (1986) were developed in an attempt to describe the radiation action on cell killing beyond the concept of the target theory. These models are of, or can be reduced under special conditions to, a linear-quadratic form (Alpen, 1998):

$$\frac{N}{N_0} = e^{-\left(\alpha_c D^* + \beta_c D^{*2}\right)} \tag{2.13}$$

where α_c and β_c are constants.

The two constants in the above equation represent groups of variables that contribute to the radiation effects. Obviously, better fit of the experimental data can be obtained by incorporating additional terms to relate the dose to the surviving fraction. However, the accuracy of the mechanistic interpretation suggested by each model relies on the underlying assumptions made by the authors.

D_{10}-value

The D_{10}-value is the dose needed to produce a 10-fold reduction of microbial population (WHO, 1999). It can be extracted from the survival curve. Shown in Figure 2.6, the D_{10}-value is equal to the difference between the dose levels D_1^* and D_2^* which corresponds to the logarithmic difference in the numbers of viable bacteria 10^4 and 10^3 in this illustration. The effectiveness of radiation treatment quantified by D_{10}-value depends on several intrinsic and extrinsic factors relating to the properties of the microorganism of interest and the details of the radiation process.

The experimental data for the construction of the survival curve can be obtained by irradiating a set of samples containing approximately the same amount of target microorganisms with different doses and employing an enumeration technique such as standard plate count to determine the number of survivors at each dose. Repetitions of the experiments are necessary to yield reliable results (Zimmerman & Battista, 2006).

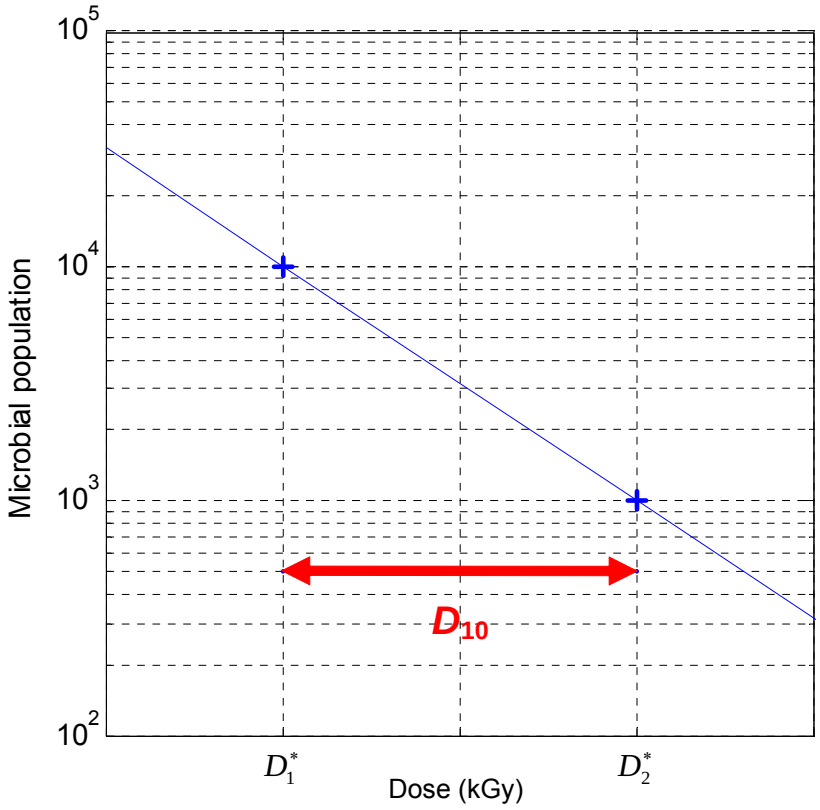

Figure 2.6. Survival curve of bacteria exposed to ionizing radiation

One of the assumptions made with the colony count methods is that each active microorganism will form a visible colony after incubation. The factors that can prevent the number of colony forming units to correctly represent the number of target microorganisms include the formation of cell clumps, the suboptimal condition for bacterial growth, the cell injury, the presence of competitive microorganisms, and other experimental errors. The number of microbial population derived from this method should only be used as an estimate (Busta, Peterson, Adams & Johnson, 1984). Because of the potential inaccuracy and the stochastic nature associated with various steps of the dose measurement and microbial enumeration, the experimental D_{10} value does carry a certain degree of uncertainty.

Application of Monte Carlo simulation in the assessment of biological damage by radiation

The Monte Carlo method is a technique of numerical analysis that employs random sampling to solve a mathematical problem (Turner, 2007). Monte Carlo track structure codes have been widely used in many research fields such as biophysical modeling, radiation protection, radiotherapy, dosimetry, radioactive beam, accelerator-driven systems, and nuclear physics. Track-structure calculation allows mechanistic studies of radiation effects despite the lack of experimental results for direct comparison. The compiled cross section data have been utilized to determine the type of interaction, mean free path, energy loss, and angle of the emitted particle for the physical events that occur as the ionizing particle traverses the medium (Nikjoo, Uehara, Emfietzoglou & Cucinotta, 2006).

In the development of the Monte Carlo track structure simulation for application in radiobiology, much emphasis was placed on the study of the physical and chemical tracks created by ionizing particles in water, the major constituent of biological tissues (Ballarini et al., 2000; Hill & Smith, 1994; Moiseenko, Hamm, Waker & Prestwich, 1998; Muroya et al., 2002; Nikjoo et al., 2006; Tomita, Kai, Kusama & Ito, 1997; Uehara & Nikjoo, 2006). Because of the importance of the spatial energy distribution, the microdosimetric approach is needed for the analysis of the molecular changes. The average quantities such as absorbed dose and equivalent dose are not adequate to describe the actions of radiation on biomolecules due to the inhomogeneous microscopic properties of the interactions (Goodhead, 2006).

A number of simulation algorithms have been formulated to investigate the impact of various ionizing agents on the target molecules (Goodhead, 2006; Nikjoo et al., 2006). In general, the simulation of radiation-induced DNA damage employs the Monte Carlo method to generate the physical tracks; from which the spatial distribution of energy deposition which leads to the evolution of the chemical tracks is obtained. The direct effect of radiation can be evaluated by calculating the amounts of energy deposited in the sensitive volumes. The indirect effect is determined by simulating the chemical reactions of the radiolysis products and the interactions between the active radicals and the cellular components.

To carry out a full Monte Carlo calculation for the assessment of biological damage from radiation, the knowledge of the cross sections for all possible interactions capable of inducing modification in the target, the probability of dissociation modes, the formation of the primary radiolytic products, and the characteristics of the chemical reactions of different radiolytic species and cellular constituents is required (Ballarini et al., 2000). To account for the consequence of the damage initially produced by the direct and indirect actions of ionizing radiation, the biological response to such damage must also be taken into consideration.

The degrees of sophistication of the track structures and the biological targets have increased over the years. The complexity of the design of molecular targets ranges from simple geometrical shapes such as cylinders to atomistic structures of biomolecules (Moiseenko et al., 1998; Nikjoo, O'Neill, Terrissol & Goodhead, 1999). The details of the calculation, e.g., the exact model of the target molecules and the probabilities of reactions of radiolytic species, differ for each model. At the moment, no one particular code developed for the determination of DNA damage is universally regarded as the most accurate and thorough model. Nevertheless, the results reported from different studies provide informative insights into the radiation response of living cells.

CHAPTER III

MODEL FORMULATION

Several physical, chemical, and biological changes in the irradiated cells occur following the absorption of radiation energy. The proposed algorithm determines the effects of energetic electrons on microbial survival by chronologically simulating a series of events induced by energy deposition. The step-by-step Monte-Carlo technique is adopted to determine the formation of damage in the DNA constituents. The resulting DNA lesions and the dose administered are used to construct the survival curve, from which the D_{10}-value is derived.

Simulation of electron transport in water

GEANT4, a toolkit which utilizes the Monte Carlo method for simulating the passage of particles through matter, is among one of the existing codes that has a comprehensive set of physics processes available for the model developer to implement in a specific design. The code was developed by a collaboration of radiation physicists and software engineers and has been applied in a variety of research projects related to radiation exposure (Agostinelli et al., 2003).

The GEANT4 electromagnetic models were systematically validated against the United States National Institute of Standards and Technologies (NIST) reference data. The total attenuation coefficients and the cross sections for the photoelectric effect, Compton scattering, and pair production of photons, as well as the stopping power and the range of electrons were found to be in good agreement with the NIST database (Amako et al., 2005). The suitability and reliability of this software package made GEANT4 the choice of toolkit used in this proposed model to generate the track structure of energetic electrons.

Calculations of cross sections and stopping powers in GEANT4

The formulae used in the GEANT4 simulation toolkit are provided below. These parameterized equations are as given in the GEANT4 physics reference manual (2007).

Cross section for photoelectric effect

The photoabsorption cross section, $\sigma_{pe}(Z,h\nu)$, is parameterized as:

$$\sigma_{pe}(Z,h\nu)=\frac{a_{pe}(Z,h\nu)}{h\nu}+\frac{b_{pe}(Z,h\nu)}{(h\nu)^2}+\frac{c_{pe}(Z,h\nu)}{(h\nu)^3}+\frac{d_{pe}(Z,h\nu)}{(h\nu)^4}. \quad (3.1)$$

The coefficients a_{pe}, b_{pe}, c_{pe}, and d_{pe} were separately least squares fitted to the experimental data in several energy intervals.

The energy of the ejected electron is determined from the atomic shell data, while the K-shell angular distribution is used to sample the direction of the electron.

Cross section for Compton scattering

The empirical cross section formula is used for simulating the Compton scattering effect:

$$\sigma_{Cs}(Z,h\nu)=P_1(Z)\frac{\log(1+2\alpha)}{\alpha}+\frac{P_2(Z)+P_3(Z)\alpha+P_4(Z)\alpha^2}{1+a_{Cx}\alpha+b_{Cx}\alpha^2+c_{Cx}\alpha^3} \quad (3.2)$$

where $\alpha=\frac{h\nu}{m_0c^2}$ and m_0 is the electron mass.

The angular distribution of the photon is determined using the quantum mechanical Klein-Nishina differential cross section per atom, $\frac{d\sigma_{KN}}{d\varepsilon}$:

$$\frac{d\sigma_{KN}}{d\varepsilon}=\pi r_e^2\frac{m_0c^2}{h\nu}Z\left(\frac{1}{\varepsilon}+\varepsilon\right)\left(1-\frac{\varepsilon\sin^2\theta}{1+\varepsilon^2}\right) \quad (3.3)$$

where r_e is the classical electron radius and $\varepsilon=\frac{h\nu'}{h\nu}$.

Cross section for pair production

The parameterized cross section per atom for the pair production process, $\sigma_{e^-e^+}(Z,h\nu)$, is calculated as:

$$\sigma_{e^-e^+}(Z,h\nu) = Z(Z+1)\left[F_1(\ln\alpha) + F_2(\ln\alpha)Z + \frac{F_3(\ln\alpha)}{Z}\right]. \quad (3.4)$$

The functions F_1, F_2, and F_3 are given as:

$$F_1(\ln\alpha) = a_{p_0} + a_{p_1}(\ln\alpha) + a_{p_2}(\ln\alpha)^2 + a_{p_3}(\ln\alpha)^3 + a_{p_4}(\ln\alpha)^4 + a_{p_5}(\ln\alpha)^5 \quad (3.5)$$

$$F_2(\ln\alpha) = b_{p_0} + b_{p_1}(\ln\alpha) + b_{p_2}(\ln\alpha)^2 + b_{p_3}(\ln\alpha)^3 + b_{p_4}(\ln\alpha)^4 + b_{p_5}(\ln\alpha)^5$$

$$F_3(\ln\alpha) = c_{p_0} + c_{p_1}(\ln\alpha) + c_{p_2}(\ln\alpha)^2 + c_{p_3}(\ln\alpha)^3 + c_{p_4}(\ln\alpha)^4 + c_{p_5}(\ln\alpha)^5$$

where a_{p_i}, b_{p_i}, and c_{p_i} are least-squares-fit parameters.

The above set of equations is applicable for $1 \le Z \le 100$ and $h\nu \in$ [1.5 MeV,100 GeV]. The $\sigma_{e^-e^+}(Z,h\nu)$ is constant above 100 GeV. For $h\nu$ < 1.5 MeV, $h\nu_{low}$, $\sigma_{e^-e^+}(Z,h\nu)$ is extrapolated by

$$\sigma_{e^-e^+}(h\nu) = \sigma_{e^-e^+}(h\nu_{low}) \times \left(\frac{h\nu - 2m_0c^2}{h\nu_{low} - 2m_0c^2}\right)^2. \quad (3.6)$$

Cross section for positron-electron annihilation

The cross section for the in-flight annihilation of a positron and a free electron is calculated by the formula of Heitler:

$$\sigma_{AN}(Z,E_{e^+}) = \frac{Z\pi r_e^2}{\gamma_{e^+}+1}\left[\frac{\gamma_{e^+}^2 + 4\gamma_{e^+} + 1}{\gamma_{e^+}^2 - 1}\ln\left(\gamma_{e^+} + \sqrt{\gamma_{e^+}^2 - 1}\right) - \frac{\gamma_{e^+} + 3}{\sqrt{\gamma_{e^+}^2 - 1}}\right] \quad (3.7)$$

where $\gamma_{e^+} = \frac{E_{e^+}}{m_0c^2}$ and E_{e^+} is the total energy of the positron.

Collision stopping power

The continuous energy losses of electrons and positrons with the energies below the δ-ray production threshold are determined from Berger-Seltzer formula:

$$\left.\frac{dE}{dx}\right]_{T<T_{cut}} = 2\pi r_e^2 m_0 c^2 n_{el} \frac{1}{\beta_{\gamma_e}^2}\left[\ln\frac{2(\gamma_e+1)}{\left(I_m/m_0c^2\right)^2} + F^{\pm}\left(\tau_{\gamma_e},\tau_{up}\right) - \delta_p\right] \tag{3.8}$$

where $\gamma_e = \frac{E}{m_0c^2}$, $\beta_{\gamma_e}^2 = 1-\left(1/\gamma_e^2\right)$, $\tau_{\gamma_e} = \gamma_e - 1$, $\tau_c = \frac{T_{cut}}{m_0c^2}$, $\tau_{up} = \min\left(\tau_c, \tau_{\max}\right)$, $\tau_{\max}$ is the maximum energy transfer, T_{cut} is the minimum energy cut for δ-ray production, δ_p is the density effect function, and n_{el} and I_m are the electron density and the mean excitation energy of the material respectively.

For positrons,

$$F^{+}\left(\tau_{\gamma_e},\tau_{up}\right) = \ln\left(\tau_{\gamma_e}\tau_{up}\right) - \frac{\tau_{up}^2}{\tau_{\gamma_e}}\left[\tau_{\gamma_e} + 2\tau_{up} - \frac{3\tau_{up}^2 y_{\gamma_e}}{2} - \left(\tau_{up} - \frac{\tau_{up}^3}{3}\right)y_{\gamma_e}^2 - \left(\frac{\tau_{up}^2}{2} - \tau_{\gamma_e}\frac{\tau_{up}^3}{3} + \frac{\tau_{up}^4}{4}\right)y_{\gamma_e}^3\right] \tag{3.9}$$

and for electrons,

$$F^{-}\left(\tau_{\gamma_e},\tau_{up}\right) = -1 - \beta_{\gamma_e}^2 + \ln\left[\left(\tau_{\gamma_e}-\tau_{up}\right)\tau_{up}\right] + \frac{\tau_{\gamma_e}}{\tau_{\gamma_e}-\tau_{up}} + \frac{1}{\gamma_e^2}\left[\frac{\tau_{up}^2}{2} + \left(2\tau_{\gamma_e}+1\right)\ln\left(1-\frac{\tau_{up}}{\tau_{\gamma_e}}\right)\right] \tag{3.10}$$

where $y_{\gamma_e} = \frac{1}{\gamma_e+1}$.

The energy losses from the production of delta rays by electrons and positrons that have the energies above the threshold are determined by Möller scattering and Bhabha scattering respectively.

The total cross section per atom for Möller scattering, $\sigma_{\text{Möller}}\left(Z,E,T_{cut}\right)$, and Bhabha scattering, $\sigma_{\text{Bhabha}}\left(Z,E,T_{cut}\right)$, are computed as:

$$\sigma_{\text{Möller}}\left(Z,E,T_{cut}\right)=\frac{2\pi r_e^2 Z}{\beta_{\gamma_e}^2\left(\gamma_e-1\right)}\times\left[\frac{\left(\gamma_e-1\right)^2}{\gamma_e^2}\left(\frac{1}{2}-x_e\right)+\frac{1}{x_e}-\frac{1}{1-x_e}-\frac{2\gamma_e-1}{\gamma_e^2}\ln\frac{1-x_e}{x_e}\right] \text{ and}$$

(3.11)

$$\sigma_{\text{Bhabha}}\left(Z,E,T_{cut}\right)=\frac{2\pi r_e^2 Z}{\left(\gamma_e-1\right)}\times\left[\frac{1}{\beta_{\gamma_e}^2}\left(\frac{1}{x_e}-1\right)+B_1\ln x_e+B_2\left(1-x_e\right)-\frac{B_3}{2}\left(1-x_e^2\right)+\frac{B_4}{3}\left(1-x_e^3\right)\right].$$

(3.12)

In the above equations, $B_1=2-y_{\gamma_e}^2$,

$$B_2=\left(1-2y_{\gamma_e}\right)\left(3+y_{\gamma_e}^2\right),$$

$$B_3=\left(1-2y_{\gamma_e}\right)^2+\left(1-2y_{\gamma_e}\right)^3,$$

$$B_4=\left(1-2y_{\gamma_e}\right)^3$$

and $x_e=\frac{T_{cut}}{\left(E-m_0c^2\right)}$.

Radiative stopping power

The energy loss of electrons due to the radiation of photons in the field of a nucleus is parameterized as:

$$E_{loss}^{brem}\left(Z,E,k_c\right)=\frac{Z\left(Z+\xi_l\right)\left(E+m_0\right)^2}{\left(E+2m_0\right)}\left[\frac{k_c}{E}\right]^{\beta_b}\left(2-c_{lh}Z^{\frac{1}{4}}\right)\frac{a_b+b_b\frac{E}{E_{\lim}}}{1+c_b\frac{E}{E_{\lim}}}\frac{f_l}{N_A} \qquad (3.13)$$

where ξ_l, β_b, c_{lh}, a_b, b_b, and c_b are constants, and f_l is a polynomial with Z–dependent coefficients.

The cross section for bremsstrahlung is calculated from the parameterization:

$$\sigma_{brem}\left(Z,E,k_c\right)=Z\left(Z+\xi_\sigma\right)\left(1-c_{sigh}Z^{1/4}\right)\left[\frac{E}{k_c}\right]^{\alpha_b}\frac{f_s}{N_A} \qquad (3.14)$$

where ξ_σ, c_{sigh}, and α_b are constants, and f_s is a polynomial with Z–dependent coefficients.

Design of the irradiated system

The simulated system is composed of the traversing electrons and the attenuating medium which represents the bacterial nucleoid. The irradiated object is a container filled with water and the DNA of the microorganisms. Only interactions taking place inside the nucleoid region are considered in the proposed model.

For the track structure calculation, the chemical composition and the density of liquid water were used to characterize the irradiated medium. The water container has a 3-dimensional rectangular shape with the cross-sectional area of 0.8 mm^2. The depth of the container was selected by running a Monte Carlo simulation for 10,000 tracks to obtain an appropriate penetration depth. This depth was predetermined to avoid the situation where large volume in the container receives no energy deposition which consequently leads to misinterpretation of the radiation effects when the degree of DNA damage is associated with the radiation dose.

More than 600,000 detectors are placed inside the container. The mean DNA volume fraction derived from the published data (Woldringh & Nanninga, 1985; Woldringh & Odijk, 1999) was used to estimate the size of the detector which would contain the average number of one DNA double helix. These detectors are arbitrarily located in systematically defined blocks. Blocks are generated to prevent the overlap of the detector volumes. Figure 3.1 partially illustrates the positioning of the detectors within a portion of the container. The blue dots indicate the detector locations. Each interval on the x-, y- and z- axes corresponds to the length of 50 nm, 20,000 nm, and 20,000 nm respectively.

In each trial of the simulation, over 6,000,000 electrons enter the container having the momentum toward the depth direction (x-axis of Figure 3.1). The energy of the incident electrons is set at 5 keV assuming that similar end results of the biological damage at the same dose levels would be observed for electron beams of higher energy. The incident electron energy was kept constant throughout the study to minimize the number of variables. To ensure the stochastic nature of the incoming electrons in each section of the medium being irradiated, the coordinates of the starting positions of incident electrons were randomly selected on the entering plane perpendicular to the direction of the beam.

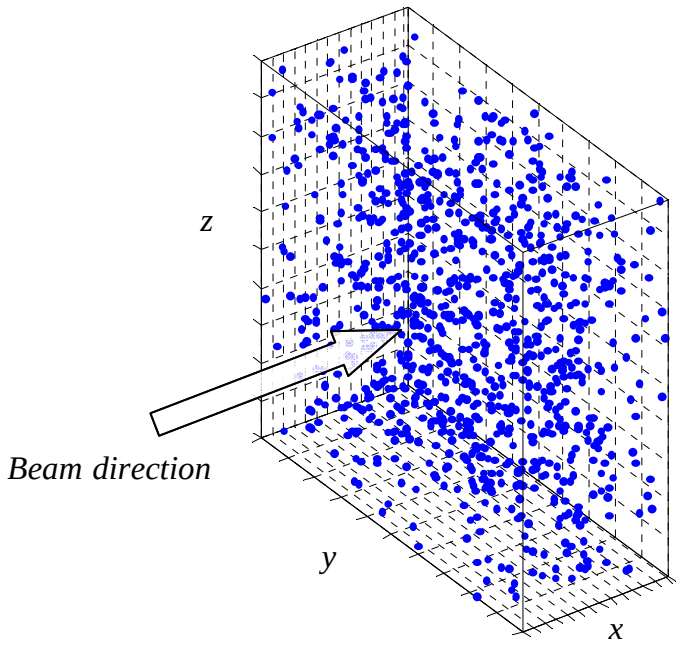

Figure 3.1. Schematic representation of the simulated radiation treatment

The information collected from GEANT4 simulation includes the identification of the detectors that contain the electron track(s), the positions of the energy deposition, the amount of deposited energy at each location, the kinetic energies of the electrons along the tracks inside the detectors, and the total energy absorption in the irradiated object. The results are converted to the compatible file format, which can be used as the input data for the subsequent step of the simulation. The codes in the following sections were written in MATLAB (Mathworks, Natick, MA).

Construction of the target molecules

B-form DNA is created inside the detector. The assumptions made regarding the volume of the detector and the structure of the DNA molecule are that DNA helices are homogeneously distributed throughout the nucleoid region and that interactions between the DNA and other substances within the nucleoid are negligible. The DNA segment is positioned in a random orientation in the detector to mimic the DNA arrangement in the cell. The two ends of the DNA molecule are forced to be on the opposite sides of the box. Figure 3.2 depicts the examples of the positions and geometries of the DNA in the detectors.

Different parts of the actual genomic sequence of *Escherichia coli* O157:H7 EDL933 (Perna et al., 2001) are arbitrarily selected as the inputs for the base sequence. Additionally, the genome of *Listeria monocytogenes* 4b F2365 (Nelson et al., 2004) was used to investigate the impact of the bacterial genome on the sensitivity to radiation damage. These genomes were retrieved from The Comprehensive Microbial Resource online database. Both *E. coli* O157:H7, a verotoxin-producing bacterium that can cause hemorrhagic diarrhea, and *L. monocytogenes*, a bacterium known to cause listeriosis, were chosen in this study because they are among the common pathogens found in foods that are subjected to decontamination by food processors. The effects of using the double helices that contain only either AT or GC base pairs were also examined.

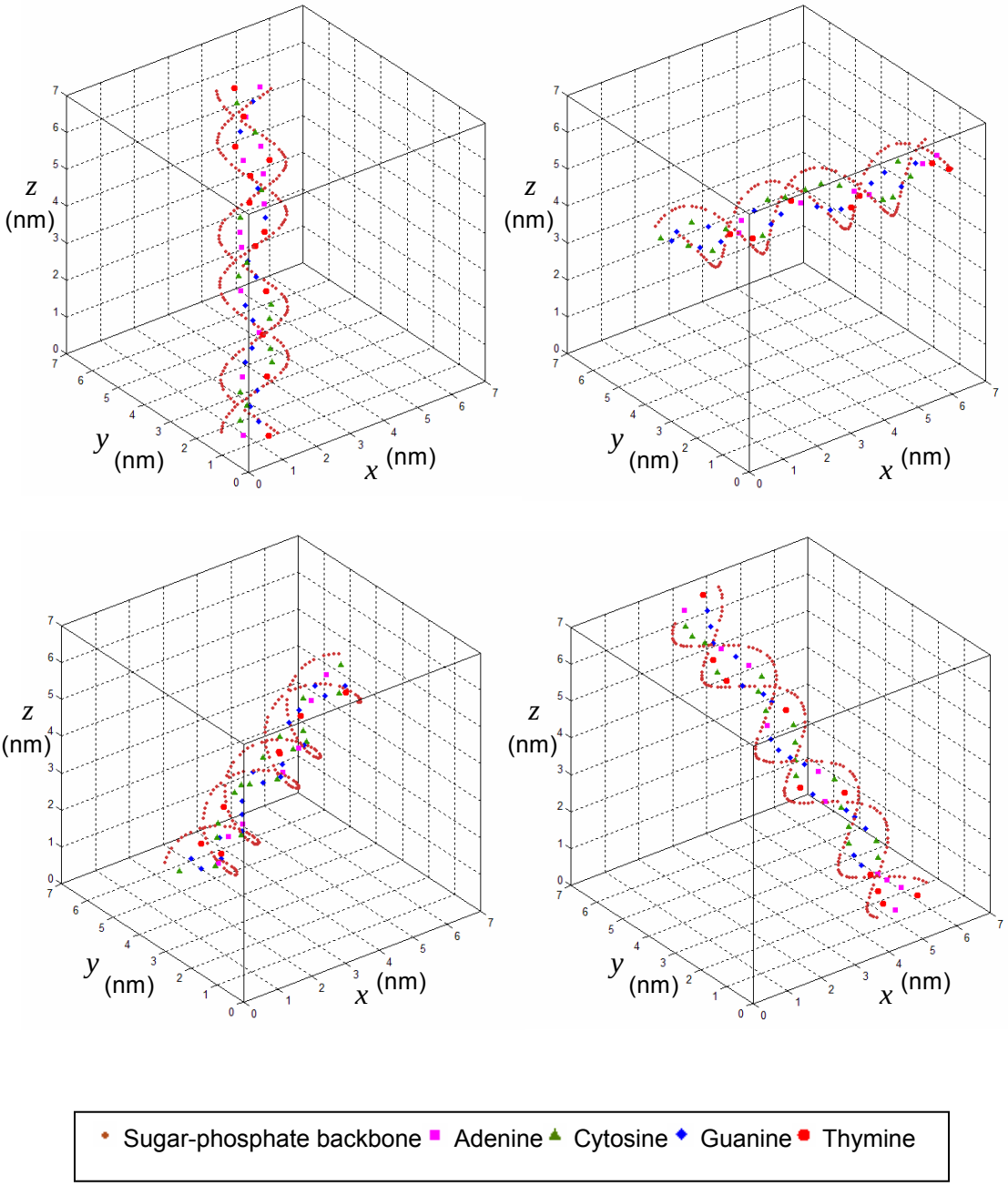

Figure 3.2. Illustrations of DNA molecules inside the detectors

Assessment of DNA damage from direct energy deposition

After the track structure is obtained and the detectors which contain the deposited energies of electrons are superimposed with the DNA, the DNA damage from direct ionization of DNA molecule is evaluated. Some modelers in the previous studies have used the presumed energy deposit thresholds deduced from the experimental data to determine whether the event of energy deposition will result in a DNA lesion (e.g., Moiseenko et al., 1998; Nikjoo et al., 1999). The linear probability function for the induction of DNA damage by the deposited energy has also been employed (Bernhardt, Friedland, Meckbach, Jacob & Paretzke, 2002). In the currently proposed model, the resulting DNA damage attributed to the direct energy deposition is assumed to be proportional to the ionization cross sections of the DNA.

Binary-Encounter-Bethe, BEB, theory is one of the formalisms that can be used to compute the electron-impact ionization cross sections of the DNA molecules. The formalism predicts the total ionization cross section as the sum of the ionization cross sections for ejecting an electron from each of the molecular orbitals without any adjustable or fitted parameter. Only simple input data for the ground state which can be obtained from standard molecular wave function codes is required for the calculation. The theory was proved to be valid for numerous molecules for the entire incident energy range from threshold to several keV (Kim, Hwang, Weinberger, Ali & Rudd, 1997). Because of its simplicity, BEB formalism was utilized in the present study to assess the direct effect of radiation.

The analytical form and input data used to calculate the BEB cross section were taken from the published paper by Bernhardt and Paretzke (2003). The equation for BEB cross section, $\sigma_{BEB-DNA}$, which represents the probability of ionization of DNA constituents in the proposed algorithm is

$$\sigma_{BEB-DNA} = \sum_j \frac{4\pi a_0^2 \xi_j \left(\frac{R}{E_j}\right)^2}{\left(\frac{E}{E_j}\right)+\left(\frac{U_j}{E_j}\right)+1} \times \frac{\ln\left(\frac{E}{E_j}\right)}{2}\left(1-\frac{1}{\left(\frac{E}{E_j}\right)^2}\right)+\left(1-\frac{1}{\left(\frac{E}{E_j}\right)}-\frac{\ln\left(\frac{E}{E_j}\right)}{\left(\frac{E}{E_j}\right)+1}\right) \quad (3.15)$$

where E is the kinetic energy of the incoming electron, a_0 is the Bohr radius (0.0529 nm), R is the Rydberg energy (13.61 eV), j is the index of the molecular subshell, E_j is the binding energy, U_j is the average orbital kinetic energy of the target electron, and ξ_j is the number of electrons in the respective orbital.

The sensitive volumes of the bases and the sugar-phosphate backbone are assumed to be spheres with the radii, $r_{BEB-DNA}$, calculated by

$$r_{BEB-DNA} = \sqrt{\frac{\sigma_{BEB-DNA}}{\pi}} \quad . \tag{3.16}$$

If the energy deposition is located in the sensitive volume of the DNA base, a base damage, BD, is produced. If the volume that contains the energy deposition is that of the sugar-phosphate backbone, then the interaction is further checked whether the damage would be a double strand break, DSB, rather than a single strand break, SSB, by reducing $r_{BEB-DNA}$ down to 50% of the original value. When the interaction occurs, the type of damage and the location on the DNA are recorded and the energy deposition that causes the lesion is removed from further consideration.

Evaluation of DNA damage by radicals from water radiolysis

The deposited energy that does not induce DNA lesion via direct ionization in the detector is used to determine the production of the radiolytic radicals. The species H_2O^+, H_2O^*, and subexcitation electrons are formed in the physical stage (~≤ 10^{-15} s) as a result of electron interactions with liquid water. These ionized and excited molecules are replaced by other radiolytic species while subexcitation electrons become hydrated after the thermalization-hydration process during the physico-chemical stage (~10^{-15} s to ~10^{-12} s) (Turner, 2007).

Ionization of the water molecule is usually assumed to cause the formation of a hydronium ion and a hydroxyl radical by a number of modelers. Not much is known about the initial production of the radiolytic species from each excited state of liquid water. Different sets of decay probabilities have been suggested. Various researchers have their own assumptions

regarding the branching ratios that would generate consistent *G*-values, the number of species produced per 100 eV of energy absorbed in the medium, for the radiolytic products. Due to the lack of sufficient experimental data, there is no consensus on which dissociation scheme is the most plausible (Uehara & Nikjoo, 2006).

In the proposed algorithm, the ionization cross section, σ_i, is calculated with the set of equations provided below (Green, 1975; Olivero, Stagat & Green, 1972):

$$\sigma_i(E) = A\Gamma\left(\tan^{-1}\left(\frac{(T_m - T_0)}{\Gamma}\right) + \tan^{-1}\left(\frac{T_0}{\Gamma}\right)\right) \tag{3.17}$$

$$T_m = \frac{1}{2}(E - I) \tag{3.18}$$

$$T_0(E) = T_s - \left[\frac{T_a}{(E + T_b)}\right] \tag{3.19}$$

$$\Gamma(E) = \Gamma_s\left[\frac{E}{E + \Gamma_b}\right] \tag{3.20}$$

$$A(E) = \left(\frac{\sigma_0 K_a}{E + K_b}\right)\ln\left(\frac{E}{J_a} - J_b\right) \tag{3.21}$$

where T_m is the maximum energy of the secondary electron, I is the ionization threshold, σ_0 is the unit cross section, and K_a, K_b, J_a, J_b, Γ_s, Γ_b, T_a, T_b, and T_s are fixed numbers.

The equation for the total ionization cross section was derived by summing up the cross sections of individual ionization processes employing the values of parameters for liquid water reported by Kutcher and Green (1976). The form of the equation is in the same format as that used by Uehara et al. (1999):

$$\sigma_{ion} = a_i t_{ion}^{r_i} e^{-\left(b_{i1} t_{ion} + b_{i2} t_{ion}^2\right)} \tag{3.22}$$

$$t_{ion} = \ln\frac{E}{d_i} \tag{3.23}$$

where the total ionization cross section of liquid water, σ_{ion} , is in Å^2, the electron kinetic energy, E , is in eV. The fitting parameters a_i , b_{i1} , b_{i2} , d_i , and r_i are 4.228, 2.168, -0.049, 10.324, and 4.285 respectively.

The cross sections for excitation processes, $\sigma_{exc}(E)$, are computed as (Olivero et al., 1972):

$$\sigma_{exc}(E) = \frac{\pi a_0^2 (2R)^2 f_o c_o}{W^2} \left(\frac{W}{E}\right)^{\Omega_{ex}} \left[1 - \left(\frac{W}{E}\right)^{\beta_{ex}}\right]^{\upsilon_{ex}} \quad (3.24)$$

where $f_o c_o$ is the overall normalization, W is the excitation energy, and Ω_{ex} , β_{ex} , and υ_{ex} are fitting parameters. The values of the parameters for the calculation of excitation cross sections were taken from the work of Kutcher and Green (1976).

The cross sections for the competing ionization and excitation processes are shown in Figure 3.3. These cross sections are used to indicate how likely each process would take place upon the deposition of energy by the incident electrons.

For the ionization process considered in the proposed model, a hydronium ion and a hydroxyl radical are produced by a reaction between an ionized water molecule and an adjacent water molecule:

$$H_2O^+ + H_2O \rightarrow H_3O^+ + OH. \quad (3.25)$$

The H_2O^+ ion migrates in a random direction after its formation with a displacement of 1.25 nm away from the site of production and is replaced by the H_3O^+. The OH radical is positioned with an arbitrary orientation at a distance of 0.29 nm which is equivalent to the diameter of a water molecule (Tomita et al., 1997).

In the excitation processes, H, OH, H_2, O, H_3O^+, and e_{aq}^- are generated from different excited states as shown in Table 3.1. Since there are some arguments against the existence of the plasmon state (LaVerne & Mozumder, 1993), it is not included in this model.

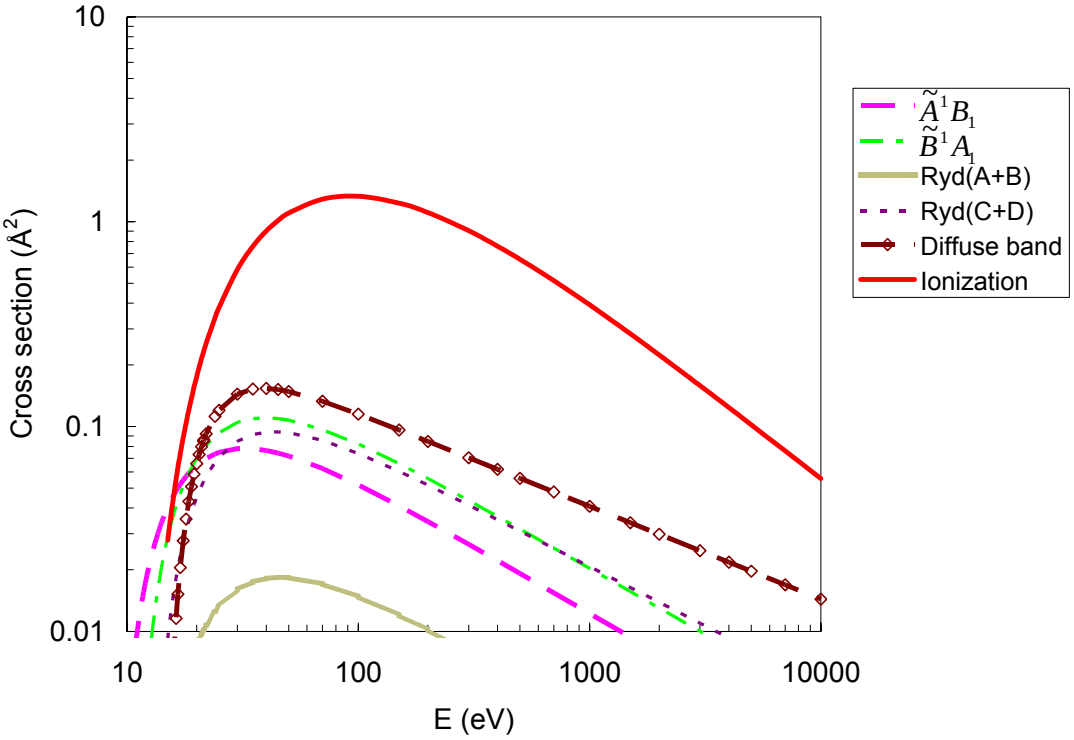

Figure 3.3. Excitation and ionization cross sections for liquid water

Table 3.1. Assumed products of different excitation states (Hill & Smith, 1994)

Excitation state	Products
$\tilde{A}^1B_1$	H + OH
$\tilde{B}^1A_1$	H_2 + O
Ryd(A+B)	$H_3O^+ + OH + e^-_{aq}$
Ryd(C+D)	$H_3O^+ + OH + e^-_{aq}$
Diffuse band	$H_3O^+ + OH + e^-_{aq}$

For the dissociation of an excited water molecule that leads to the formation of the H and OH radicals, the products are placed 0.87 nm apart. When H_2 and O are produced, they are separated by 0.58 nm. In both cases, the species are located on a randomly oriented line centered at the site of the excited water molecule (Hill & Smith, 1994). O is assumed to combine with H_2O to form H_2O_2 (Moiseenko et al.,1998). The hydrated or aqueous electron, e^-_{aq}, is placed

in a random orientation at a distance of 0.65 nm, the most probable value of the thermalization distance (Muroya et al., 2002), from the production site.

After the formations of the radiolytic species at the end of the physico-chemical stage are determined, these species are checked whether they would react with the DNA constituents or one another by means of diffusion-controlled reactions (Aydogan, Bolch, Swarts, Turner & Marshall, 2008) in the chemical stage (~10^{-12}s to ~10^{-6}s) (Turner, 2007). All species are assumed to diffuse randomly in the medium and interact when the separation distance is less than the reaction radius for the respective reaction.

The reaction radius for the radical reaction with the DNA constituent is obtained by using Smoluchowski's diffusion equation:

$$k_d = 4\pi N_A (D_a + D_b) r_{ab} \tag{3.26}$$

where k_d is the diffusion-controlled reaction rate constant, N_A is the Avogadro's number, D is the diffusion constant with the subscripts a and b representing 2 different species, and r_{ab} is the reaction radius.

The diffusion constants for DNA constituents are set to zero because the DNA is relatively stationary in the cell compared to other water radicals (Aydogan et al., 2008; Moiseenko et al., 1998). Among all radiolytic species, the hydroxyl radical and the hydrated electron are considered to be capable of producing damaged bases. For the damage to the sugar backbone, a DNA strand break can only be induced by the hydroxyl radical (Moiseenko et al., 1998).

When the OH radical and the e_{aq}^{-} are generated, they are checked whether their locations are close enough to react with any of the DNA constituent. The reaction rates used in the proposed model are provided in Table 3.2. If any reaction with the DNA occurs, the type and location of the damage are recorded. The distance between any two closest radiolytic species is then determined and compared with the reaction radius given in Table 3.3. If no reaction takes place, each species is allowed to jump at a distance according to its diffusion coefficient shown in Table 3.4 in a random direction until the next time step.

Table 3.2. Reaction rate constants for the reactions of the water radicals with the sugar moiety and the nucleobases (Aydogan et al., 2008)

Water radical	DNA constituent	Reaction rate constant (10^9 M^{-1} s^{-1})
OH	Deoxyribose	2.50
	Adenine	6.10
	Cytosine	6.10
	Guanine	9.20
	Thymine	6.40
e^-_{aq}	Adenine	9.00
	Cytosine	13.00
	Guanine	14.00
	Thymine	17.00

Table 3.3. Reaction radii for the set of water radiolysis reactions (Hamm, Turner & Stabin, 1998)

Reaction	Reaction radius (nm)
$H + OH \rightarrow H_2O$	0.43
$e^-_{aq} + OH \rightarrow OH^-$	0.72
$e^-_{aq} + H + H_2O \rightarrow H_2 + OH^-$	0.45
$e^-_{aq} + H_3O^+ \rightarrow H + H_2O$	0.39
$H + H \rightarrow H_2$	0.23
$OH + OH \rightarrow H_2O_2$	0.26
$2\,e^-_{aq} + 2H_2O \rightarrow H_2 + 2OH^-$	0.18
$H_3O^+ + OH^- \rightarrow 2H_2O$	1.58
$e^-_{aq} + H_2O_2 \rightarrow OH + OH^-$	0.40
$OH + OH^- \rightarrow H_2O + O^-$	0.36

Table 3.4. Diffusion constants for individual species (Hamm et al., 1998)

Species	D (10^{-5} cm^2s^{-1})
H	8.0
OH	2.5
e^-_{aq}	5.0
H_3O^+	9.5
OH^-	5.3
H_2O_2	1.4

The jump size λ for time step τ is

$$\lambda = \sqrt{6D\tau}\,. \tag{3.27}$$

To eliminate the possibility that any two species could be in a closer proximity than their initial and final positions for each time step, the minimum separation distance, $r_{\min}$, is computed at the end of each jump (Hamm et al., 1998):

$$r_{\min} = \sqrt{\left(x_{20} - x_{10} + (\varpi_2 - \varpi_1)\frac{t_{\min}}{\tau}\right)^2 + \left(y_{20} - y_{10} + (\eta_2 - \eta_1)\frac{t_{\min}}{\tau}\right)^2 + \left(z_{20} - z_{10} + (\zeta_2 - \zeta_1)\frac{t_{\min}}{\tau}\right)^2} \tag{3.28}$$

where (x_{10}, y_{10}, z_{10}) and (x_{20}, y_{20}, z_{20}) are the coordinates of the initial positions of the two species, the quantities ϖ, η, and ζ are the displacements in the three coordinate directions after time τ, and $t_{\min}$ indicates the time at which the diffusing species are minimally separated:

$$t_{\min} = \left[\frac{(x_{10} - x_{20})(\varpi_2 - \varpi_1) + (y_{10} - y_{20})(\eta_2 - \eta_1) + (z_{10} - z_{20})(\zeta_2 - \zeta_1)}{(\xi_2 - \xi_1)^2 + (\eta_2 - \eta_1)^2 + (\zeta_2 - \zeta_1)^2}\right]\tau\,. \tag{3.29}$$

If 'jump through' happens, i.e., $0 \le t_{\min} \le \tau$, then $r_{\min}$ is compared against the reaction radius to determine whether the chemical reaction would take place.

If any reaction between a pair of species previously located at the positions (x_{10}, y_{10}, z_{10}) and (x_{20}, y_{20}, z_{20}) occurs, the x-coordinate of the reaction site is determined by

$$x_r = x_{10}\left(\frac{\sqrt{D_2}}{\sqrt{D_1} + \sqrt{D_2}}\right) + x_{20}\left(\frac{\sqrt{D_1}}{\sqrt{D_1} + \sqrt{D_2}}\right). \tag{3.30}$$

The y- and z-coordinates are calculated in the same manner (Tomita et al., 1997).

For the chemical reactions which result in the formation of a single product, the location of the product is assumed to be at the reaction site. When more than one product is formed, the location of each product away from the reaction site is estimated by using its diffusion coefficient. τ was set at 3 picoseconds in all calculations.

To account for the scavenging effect in the cellular environment, the characteristic absorption time of $6x10^{-10}$ s, the time in which the radicals are reduced by e^{-1} (Chatterjee & Holley, 1991), is used to compute the probability that the radicals will be absorbed at the end of each time step. The effect of different scavenging capability was also investigated in this study.

The simulation cycle during the chemical stage is repeated until 10^{-6}s, the time by which the radiolysis species are either reacted with other species and become inactive or located relatively far from one another (Turner, 2007) and the DNA molecules (Moiseenko et al., 1998).

A DSB can arise from the occurrence of two or more SSB on opposite DNA strands that are close enough such that the Van der Waals forces and the hydrogen bonds between the bases can no longer hold the two strands together (Alpen, 1998). Base damages on the nearby locations on the two opposed strands could also lead to a DSB by the excision repair processes (Chang, Zhang, Takatori, Tachibana & Yonei, 2005). For the first estimate, a DSB is produced when the separation between any pair of SSB and BD on opposite strands is not greater than 10 base pairs. However, different values of the maximum number of base pairs, n_{bp}, within which different combinations of DNA damages would result in the formation of DSB, were used to evaluate the impact on the calculated D_{10}-value.

To generate meaningful representative results, each detector that contains the energy deposited by irradiation was subjected to 10,000 trials of computer simulation. A newly created DNA molecule replaces the old one in every run to imitate the nature of the DNA arrangement in the irradiated cell.

Determination of D_{10}-value from the resulting DNA damage

Once the DNA lesions due to both the direct and indirect effects are evaluated and the number of each type of DNA damage is finalized, the cell survival curve is constructed to illustrate the impact of radiation on microbial inactivation. Excel (Microsoft, Seattle, WA) was employed to plot the graphs and calculate the slopes of the survival curves.

The amount of energy deposited in the container is the difference between the summations of the energies of the electrons entering and leaving the container. The radiation dose $D_{\times}^{*}$ is the total energy deposit divided by the mass of the container.

The number of DSB from the previous step is proportionally converted to the expected number of DSB in the container, DSB_{con}. The total number of DSB in the nucleoid region of the cells of the entire bacterial population is

$$DSB_{nuc} = \frac{V_{nuc}}{V_{cell}} \times DSB_{con} \tag{3.31}$$

where V_{cell} is the volume of a bacterial cell and V_{nuc} is the nucleoid volume in a single cell.

The number of DNA lesions, which correlates to the number of events of energy deposition, was assumed to follow a Poisson distribution (Rossi & Zaider, 1996). Poisson calculation with the level of significance of $p < 0.05$ is employed to determine whether the numbers of DSB are significantly different. Since DSB is the crucial parameter that dictates cell survivability, if the two values of DSB are found to be statistically different, the corresponding D_{10}-values will be considered significantly different as well.

The number of the initial population of unirradiated cells, N_0, is calculated as:

$$N_0 = \frac{V_{con}}{V_{cell}} \tag{3.32}$$

where V_{con} is the volume of the container.

The determination of the initial microbial population which corresponds to the number of calculated DSB enables the boundary condition to be created. Since the reduction of the viable population of bacteria by ionizing radiation was postulated to be logarithmic, the size of the container and the actual number of the initial population should not affect the D_{10}-value if the administered dose is uniformly distributed.

The lethal probability is computed as:

$$P_{lethal} = \left(\frac{DSB_{nuc}}{G_{eq} \times N_0} \right)^{G_{eq}} \tag{3.33}$$

where G_{eq} is the number of genome equivalents.

When at least one copy of the entire genomic sequence is available, the injured cell has a good chance to fully recover. In order to completely inhibit the cell division, one or more DSB must be present in all of the existing genomes inside the cell. The above equation accounts for the effect of having extra copies of the genetic material on the radiation resistance. Under normal conditions, the value of 3 which represents the average value of G_{eq} of the microbial population is assumed in the calculations.

The survival probability is therefore

$$P_{survival} = 1 - P_{lethal} \, . \tag{3.34}$$

For the subsequent calculation at the next dose level, the dose is increased with a constant increment of $D_{\times}^{*}$. The same algorithm is employed to determine microbial survival with the modification in the calculation of the total number of DSB in the nucleoid regions. At the ith dose level, the number of DSB in the nucleoids is

$$DSB_{nuc}^{i} = DSB_{nuc}^{i-1} + DSB_{nuc}^{1} \times P_{survival}^{i-1} \, . \tag{3.35}$$

As the container receives higher radiation dose, the chance that the lethal damage will occur in the already inactivated cells increases. To avoid overestimation of the killing effect, the probability of such occurrence is implicitly deducted from P_{lethal}^{i}. The DSB_{nuc}^{i} in the above equation is hence not the actual number of DSB expected to be found at a certain dose but the number of DSB that can be used to determine the relative amount of clonogenically dead cells in the proposed algorithm.

The calculation of the survival probability is repeated for each linear dose increment until DSB_{nuc}^{i} approaches the value of $G_{eq} \times N_0$. The survival curve is generated by plotting the survival probability against the radiation dose. The D_{10}-value is determined as the negative inverse slope of log(survival probability) vs. dose at the linear portion of the survival curve.

The computational model developed in this study for the derivation of the D_{10}-value is summarized in the flow chart shown in Figure 3.4.

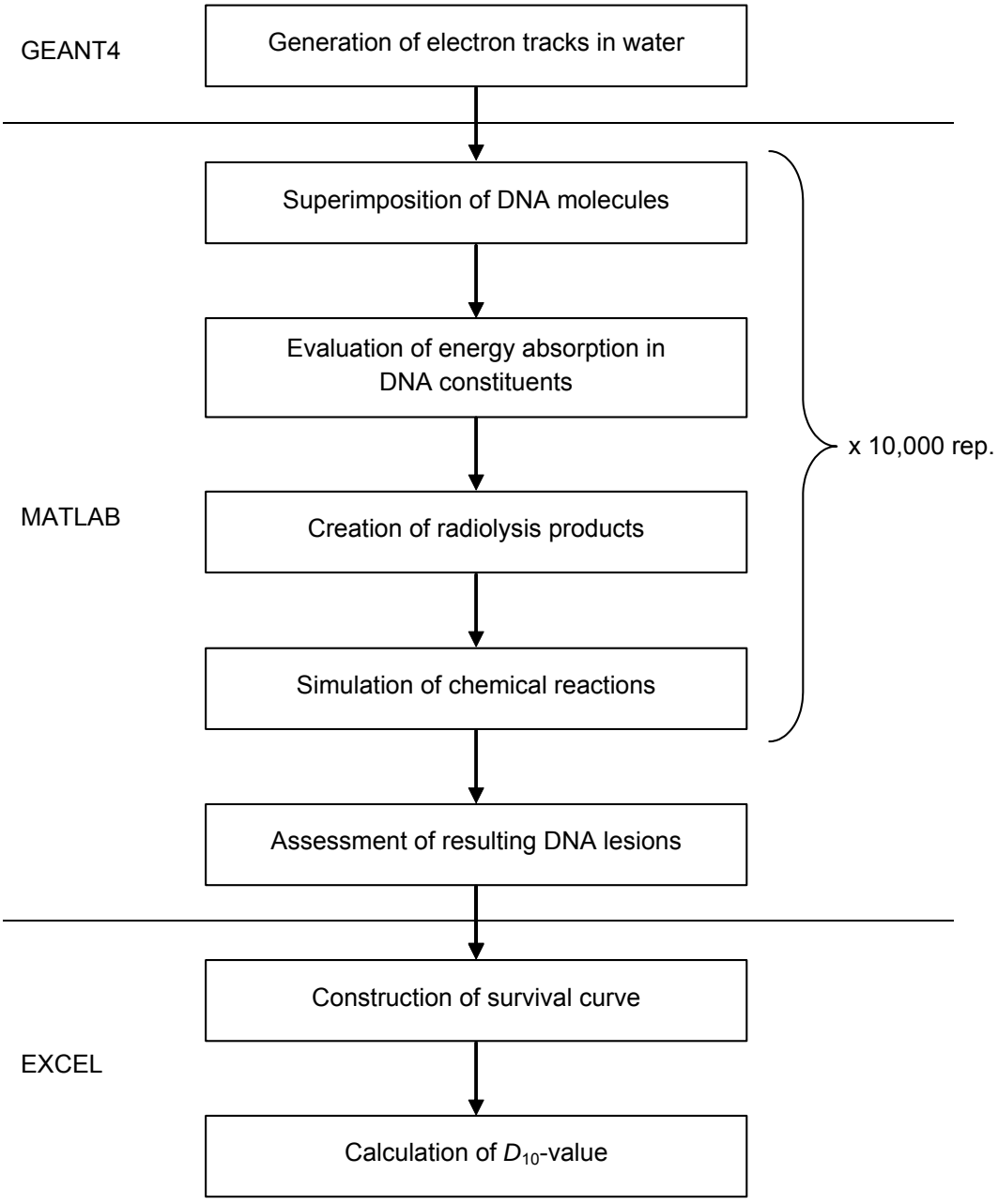

Figure 3.4. Flow chart for the determination of D_{10}-value

CHAPTER IV

RESULTS AND DISCUSSION

D_{10}-value of *E. coli* O157:H7 EDL933

The proposed model was validated by comparing the D_{10}-value of *E. coli* O157:H7 EDL933 calculated in this study with that from the published experimental result. This particular microorganism was used because the experimental D_{10}-value and the complete genome were available. The numerical comparison shows that the D_{10} value of *E. coli* O157:H7 EDL933 obtained from the developed algorithm, which was determined to be 0.357 kGy, is more than double the experimental value of 0.13 kGy reported by Rodriguez et al. (2006).

Since the ability of the microorganism to withstand radiation exposure is known to be influenced by numerous factors including the nature of the subject species, the food composition, and the condition of the radiation treatment (Sommers, 2003), to minimize the impact of such parameters, the comparison was specifically made with the experimental result of the same strain of microorganism irradiated at room temperature (20^{o}C) under normal atmospheric pressure. In addition, given that the irradiated medium used in the experiment is a model food system (10% w/w gelatin) in which water is the major component, the track structure of electrons in pure liquid water is presumably an excellent representative of that in homogenous gel, especially, at the macroscopic level, and consequently, to a lesser extent, at the molecular level.

Despite the fact that the D_{10} value resulted from the proposed model appears to be significantly higher than that of the experimental study, the agreements or disagreements between the theoretical and experimental results do not always prove the superior accuracy of either method. Certainly, the theoretically calculated D_{10} value can be altered by parameter adjustment. On the other hand, the uncertainties incurred in various steps of the experimental procedure such as dose measurement and microbial enumeration can potentially cause the resulting D_{10} value to fluctuate appreciably. Nevertheless, validation of the result generated from a newly developed approach to those from previous studies is imperative.

The D_{10} values of *E. coli* O157:H7 in various food media irradiated under diverse conditions reported in the literature are normally in the order of hundreds of gray (Ahn et al., 2006; Borsa, Lacroix, Ouattara & Chiasson, 2004; ICMSF, 1996; Levanduski & Jaczynski, 2008; Monk, Beuchat & Doyle, 1995; Niemira, 2003; Sommers, 2003). Further crude comparison with the published data suggests that the combination of theoretical models and chosen input parameters employed in this study can be used to generate a D_{10} value of reasonable magnitude.

With this level of complexity associated with the biological response to ionizing radiation, the combined effects of simultaneous changes in more than one parameter may lead to misinterpretation of the results. Conversely, individual analysis of the impact that each of the important variables has on the radiation resistance of the cell through the use of this model could provide beneficial insights into the irradiation process. Therefore, the effects of different parameters on the cell's sensitivity to radiation were examined separately in the following sections.

Effect of the bacterial genome

To evaluate the extent to which the genomic sequence can influence the killing effect of radiation, different genomes were utilized as inputs to generate the DNA sequences in the detectors. The resulting D_{10} values using the genomes of *E. coli* O157:H7 and *L. monocytogenes* as well as the two DNA sequences, each composed of only AT or GC base pairs, are presented in Table 4.1. The % DNA lesions resulted from direct ionization, which signify the relative amount of damage caused by energy deposition in the DNA molecule to the total DNA damage of a particular type, and the ratios between different kinds of DNA damage, which provide information on the relative quantity of each type of DNA lesion, are also given. Except for the input data for the base sequence, the same sets of parameters specified in the previous chapter were employed. The corresponding survival curves are shown in Figure 4.1. The slopes at the linear portion of the curves are directly translated into the D_{10} values; the steeper the slope, the lower the D_{10} value.

Table 4.1. The percentages of DNA lesion resulting from the direct effect, the damage ratios, and the calculated D_{10} values for the cells with different DNA sequences

DNA sequence	% GC content	% DSB direct	% SSB direct	% BD direct	SSB / DSB	BD / DSB	BD / SSB	D_{10} (kGy)*
E. coli O157:H7	50.38	25.00	5.27	0.90	23.52	57.04	2.43	0.357 [a]
L. monocytogenes	38.04	28.86	5.25	1.02	25.12	58.36	2.32	0.373 [ab]
Poly(AT)	0.00	34.14	4.81	1.29	28.85	56.92	1.97	0.406 [b]
Poly(GC)	100.00	22.28	5.72	0.91	20.86	59.29	2.84	0.340 [a]

* The D_{10} values that do not share the same superscript letter are significantly different ($p < 0.05$).

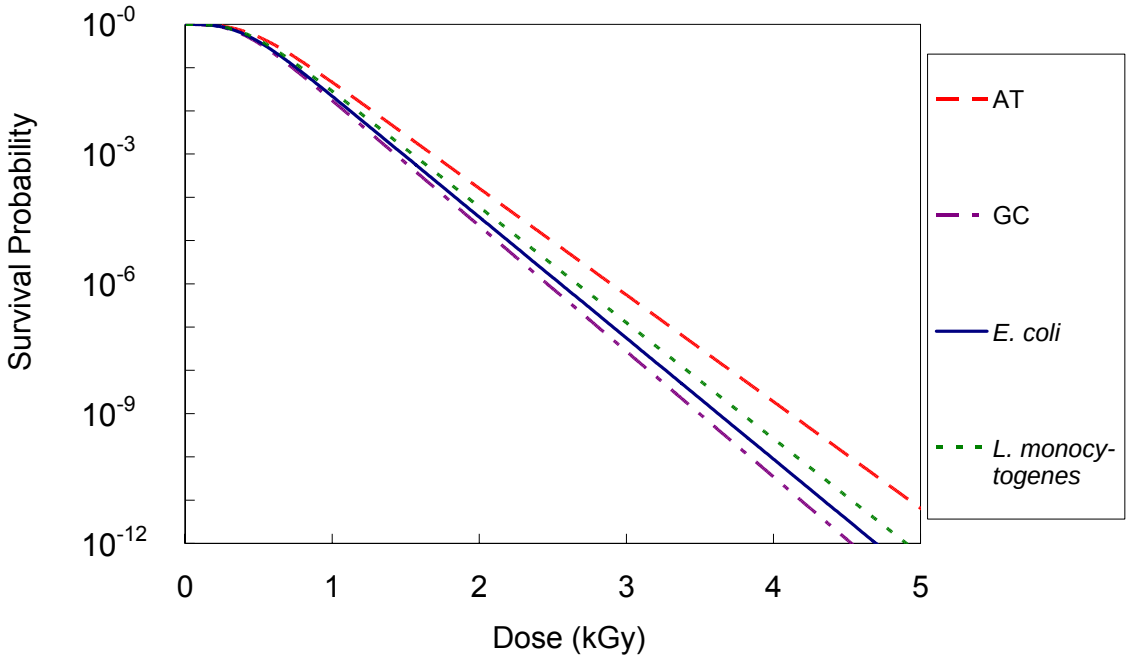

Figure 4.1. Survival curves of the cells containing different DNA sequences

The calculated fractions of DNA damage induced by energy absorption indicate that the direct-type DNA lesions constitute only a small portion of the total damage. The dominance of the indirect effect is most prominent in the case of BD, where about 99% of total BD resulted from reactions with water radicals. The degree of dominance becomes slightly smaller in the case of SSB, which could be because one of the two main radicals that can attack the nitrogenous base, the e_{aq}^{-}, does not produce significant damage to the sugar-phosphate backbone. Furthermore, the electron impact ionization cross section of the sugar-phosphate backbone is generally higher

than that of the nitrogenous base. In the induction of DSB, the relative contribution of the direct effect is much greater than those found in the productions of SSB and BD (>22% as opposed to <6 and 2%).

The differences among the relative contributions of direct ionization suggests that though the elementary damages (SSB and BD) are mostly produced by reactions with reactive water radicals, a significant portion of the lethal damage (DSB) is generated by interaction with ionizing particles. The disagreements regarding the relative contributions of the direct and indirect effects exist in the literature, not only which mechanism dominates, but also to what extent (Moiseenko et al., 1998; Nikjoo, Bolton, Watanabe, Terrissol, O'Neill & Goodhead, 2002; Nikjoo et al., 1999; Nikjoo, O'Neill, Goodhead & Terrissol, 1997; Sommers, 2003). The outcome of this study supports the argument that greater part of the radiation-induced DNA damage under normal cellular conditions is attributable to the indirect action of ionizing radiation.

The ratios between different types of DNA damage imply that BD is the most prevalent form of DNA lesion, followed by SSB and DSB. The results obtained from this proposed model are in reasonable agreement with published studies in which the amounts of DNA damage induced by energetic electrons of various energies were evaluated (Nikjoo et al., 1997; Nikjoo et al., 1999; Nikjoo et al., 2002). However, these ratios can vary to a great extent depending on the exact details of the model formulations or the experimental studies.

The variation in the genetic composition alone using the chosen set of parameters can result in the range of determined D_{10} values from 0.340 (100% GC content) to 0.406 kGy (100% AT content). A 4.5% increase in the D_{10} value is obtained when the genome of *L. monocytogenes* is used instead of the genome of *E. coli* O157:H7. Because the calculation of the D_{10} value for the genomic sequence of *L. monocytogenes* did not take into account any differences in the morphological aspects between *E. coli* O157:H7 and *L. monocytogenes*, these two D_{10} values should be regarded as those of the same type of cell differing only in the containing genetic material. Nevertheless, the results support the argument that *L. monocytogenes* is expected to be more radioresistant than *E. coli* O157:H7 which is in accordance with the experimental finding (Rodriguez, Castell-Perez, Ekpanyaskun, Moreira & Castillo, 2006).

Though, the statistical analysis indicates that some D_{10} values associated with different genetic compositions are not significantly different from one another, overall, the comparison suggests that the radiation sensitivity of a bacterium decreases with lesser GC content. The cell's ability to function against the attacks of harmful agents can be regulated by many interrelated factors. To be specific, the influence of the bacterial genome on the radiation resistance discussed here only considered the DNA damage as a consequence of radiation actions on the DNA molecules from the instance at which the radiant energy is first deposited onto the DNA up to the time by which the reactions between the DNA molecules and the radiolytic species are completed with a crude approximation of the additional DSB formation from the repair process.

Due to the fact that in the Watson-Crick DNA structure, only two types of base pairs can be accommodated, and that if the damage occurs in a particular nitrogenous base, its complementary base will also be affected, the analysis of the lesions to assess the radiation effects on the nucleobases was performed for each type of base pair (AT or GC) instead of individual bases (A, C, G, and T). Furthermore, the DNA lesions resulting from the direct and indirect actions of radiation were evaluated separately to determine the level of contribution of each effect.

In the proposed algorithm, the degree of DNA damage attributable to the direct action of radiation is governed by the values of electron impact ionization cross sections of DNA. The average ionization cross sections per base molecule of the AT and GC base pairs calculated from the Binary-Encounter-Bethe (BEB) model are provided in Figure 4.2. When the average cross sections of G and C are compared to those of A and T, BEB formalism shows that the AT base pairs are slightly more prone to radiation damage by direct energy deposition. However, for most part of the electron energy range, the ionization cross sections for both types of base pairs appear to be essentially the same. Therefore, the number of base damages due to the direct action of radiation, BD_{di}, is not expected to be significantly affected by the base composition.

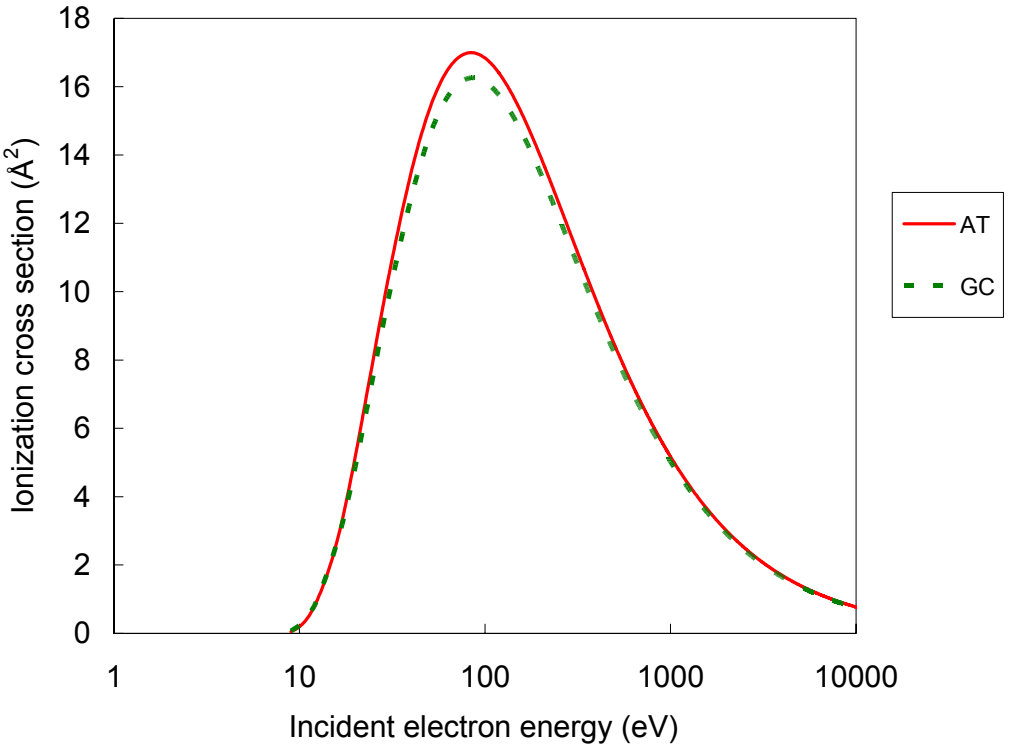

Figure 4.2. Average values of electron impact ionization cross sections for the DNA bases

Unlike the case of direct ionization, the reaction radii used in the calculation to determine the quantity of DNA damage as a result of interactions with radiolytic species are independent of the incident electron energy. The average values of the reaction rate constants for the GC base pair are greater than those for the AT base pair whether the reactions considered are with the OH or the e_{aq}^{-}. The ratios of the average reaction rate constants for G+C and A+T reacting with OH and e_{aq}^{-} are 1.22 and 1.04 respectively. For that reason, the GC base pairs are more vulnerable to attack by water radicals than are the AT base pairs. Consequently, the amount of base lesions generated by the radical mediated mechanism, BD_{in}, would be enhanced with higher GC content.

Because of the strong dominance of the indirect action of radiation in the production of BD, the effect of the genomic composition on the total number of BD is approximately the same as that on the number of BD_{in}. The overall relative contribution of the direct action of radiation is expected to be lower for the DNA sequence that has higher fraction of GC base pairs due to the greater amount of BD_{in}. Apart from the relative contribution of the direct effect in the case of pure

GC sequence, this trend is observed in the results provided in Table 4.1. The unexpected observation is very likely to be attributable to the uncertainty associated with the proposed model.

In the case of the damage to the sugar backbone that produces SSB, the indirect effect also dominates, but in contrast to the case of base damage, the portion of the total amount of SSB that is caused by direct ionization seems to increase with GC content. In fact, the actual quantity of the direct-type SSB, SSB_{di}, should not be dependent on the genomic composition because the type of the base used in the formation of BD_{di} has negligible impact on the nature of the interaction between the radiant energy and the deoxyribose-phosphate backbone. However, the number of SSB resulted from the reactions of the OH radicals, SSB_{in}, should be smaller due to the hindrance posed by the greater concentration of bases with larger reaction radii in the higher GC content sequence. As a result, % SSB induced by direct ionization are greater for the genomes that contain higher GC fractions. Therefore, the trend observed in the results is logical.

Another point that should be added to the discussion of the relative contribution of the DNA damage in the cases of SSB and BD is that a fraction of each type of DNA lesion, i.e., BD_{di}, BD_{in}, SSB_{di}, and SSB_{in}, that is attributed to the induction of DSB was deducted from the amount originally generated by ionizing radiation. Nonetheless, the magnitude of the reduction in the initial damage should be proportional to the quantity of each type, e.g., less BD_{di} in comparison to BD_{in}, and likewise, less SSB relative to BD, would be transformed into DSB. In addition, the ratios of different DNA lesions indicate that the total number of DSB is much less than that of either SSB or BD, which implies that only minute portions of SSB and BD were employed in the production of DSB. Therefore, the argument made above regarding the rationale behind the relative contribution of direct ionization still remains valid.

The same explanation that the composition of the DNA sequence has insignificant impact on the numbers of BD_{di} and SSB_{di} also applies to the formation of DSB by direct energy deposition, DSB_{di}. On the contrary, the generation of DSB from clustered damage sites, DSB_{cl}, depends on the quantities of SSB and BD available. Thus, the effect of the genomic sequence on the amount of DSB is attributed to the combined effect of the GC composition on the induction of SSB and BD. For each percent increase in the GC content, the chance that more BD can be

induced is higher than the chance that the production of SSB would be hindered; the effect of increasing the number of BD is likely to overcome the opposite effect of decreasing the number of SSB. Hence, the total number of SSB and BD would be greater allowing more DSB_{cl} in the higher GC content genome to be produced. The trend of decreasing D_{10} values resulting from the enhancement of radiation sensitivity by increasing the concentration of GC base pairs is, therefore, rational; the more the DSB generated, the smaller the D_{10} value.

With the increasing trends of DSB and BD and the decreasing trend of SSB, the decrease in the ratio of SSB/DSB and the increase in the ratio of BD/SSB due to the increase in the GC content can be automatically assumed because the numerators and the denominators of these ratios head in the opposite direction. However, for the ratio of DSB/BD, both DSB and BD are produced in greater amounts in the genome that has higher fraction of GC base pairs. The trend of this ratio thus also depends on the magnitudes of the relative changes in the BD and DSB as a function of the GC concentration. The general increase in the ratio of BD/DSB found when the sequence containing higher GC content is used in the calculation suggests that the relative increase in the amount of BD is greater than that of DSB. The only exception in the results is observed when the BD/DSB ratio for the *E. coli* O157:H7 genome is compared to that for the *L. monocytogenes* genome, in which case, the small level of inconsistency is most likely attributed to minor deviations of the results from the true means.

Not only do the genomes presented in Table 4.1 differ from one another in their genetic compositions, they also possess unique genomic sequences. To focus on the effect of the genome in terms of the primary structure of DNA, i.e., the order of nucleotides in the DNA, the inequality in the GC content was controlled by using the three different DNA sequences in the calculations: (1) the known sequence of *E. coli* O157:H7; (2) the randomly generated genomic sequence having about the same fraction of GC base pairs; and (3) the repeated sequence DNA, poly(AG), which contains approximately the same GC concentration but is arranged in the specific order. The 95% confidence intervals for the resulting D_{10} values corresponding to the three sequences are provided in Table 4.2.

Table 4.2. 95% confidence intervals for the D_{10} values of the cells with similar GC composition

DNA sequence	95% CI of the D_{10} value	
	Lower limit (kGy)	Upper limit (kGy)
E. coli O157:H7	0.328	0.389
Random	0.317	0.375
Poly(AG)	0.333	0.395

The statistical analysis yielded no significant difference which indicates that the order of the bases in the genome has negligible impact on the outcome of the simulation. With the exception of the repeating sequence polymer, the portions of the DNA sequences actually employed in the simulation could, to some extent, deviate from the specified GC composition. Nevertheless, these deviations are unlikely to be sufficient to overturn the results should a different conclusion that the radioresistance of the cell also depends on the sequence of the nucleotides rather than the base composition alone be reached.

Effect of n_{bp} and the method of DSB induction

The value of n_{bp} is associated with the strength of chemical bonds necessary to hold the double helix together and the lengths of the DNA strands involved in the DNA repair processes. The former physical meaning deals with the ability of the DNA to endure radiation damage to the point before the two DNA strands come apart. The latter takes into account the complexity of different repair pathways and the probability of the incidence that causes the two strands to eventually separate, e.g., the operation of repair enzymes on the clustered DNA damage sites that create a moment in which both strands are cut. In both cases, n_{bp} can be perceived as the quantitative parameter that represents the critical number of base pairs used to decide whether the sublethal lesions in the form of SSB (or BD) that occurred in a close proximity would lead to the formation of a DSB.

The D_{10} values are derived from the total numbers of DSB which include the DSB induced by single direct ionization (DSB_{di}) and the DSB produced by conversion of two damage sites on the opposite strands within the distance of n_{bp} (DSB_{cl}). The SSB and BD that constitute a DSB_{cl} can be introduced either by direct energy deposition of energetic electrons or by attacks of radiolytic radicals. The two methods employed to generate DSB_{cl} in the proposed model are the

SS and SB methods. In the SS method, a DSB_{cl} is only formed from a pair of SSB, whereas in the SB method, a DSB_{cl} can result from any combination of SSB and BD. The degree to which the calculated D_{10} values depend on n_{bp} and the choice between these two methods was investigated. The D_{10} values of *E. coli* O157:H7 obtained from different scenarios are given in Table 4.3.

Table 4.3. The percentages of DSB due to direct ionization, the damage ratios, and the calculated D_{10} values of *E. coli* O157:H7 for different combinations of n_{bp} and the method of DSB induction

n_{bp}	SS method (Only Combination of SSB)					SB method (Any Combination of SSB and BD)				
	% DSB direct	SSB / DSB	BD / DSB	BD / SSB	D_{10} (kGy)	% DSB direct	SSB / DSB	BD / DSB	BD / SSB	D_{10} (kGy)
0	100.00	94.41	233.84	2.48	1.461	48.95	46.22	113.45	2.45	0.710
5	99.29	93.73	232.18	2.48	1.450	30.37	28.62	69.67	2.43	0.436
10	98.59	93.06	230.55	2.48	1.440	25.00	23.52	57.04	2.43	0.357
15	97.22	91.74	227.35	2.48	1.420	22.54	21.18	51.28	2.42	0.321
20	96.55	91.09	225.78	2.48	1.410	20.96	19.65	47.56	2.42	0.298
25	96.55	91.09	225.78	2.48	1.410	20.26	18.98	45.93	2.42	0.288

The results show that the calculated D_{10} values can vary several-fold upon changing the value of n_{bp} and the algorithm used to determine the induction of DSB_{cl}. Under the circumstance that BD and SSB, as opposed to only SSB, can be utilized in the formation of DSB, the number of DSB generated by the same radiation dose is much higher. For each corresponding n_{bp}, the relative contribution of direct ionization to the total DSB production in the SB method is less than half of that in the SS method. The differences become greater with increasing n_{bp}.

Regardless of the method used to determine DSB_{cl}, as n_{bp} increases, the relative contribution of DSB from direct energy deposition decreases, with the exception of the two highest values of n_{bp} in the SS method. In which case, the calculated results seem to be saturated under the given conditions. The quantity of DSB_{di} remains the same for all the reported D_{10} values in Table 4.3, whereas the change in the calculated D_{10} value is directly related to the change in the number of DSB_{cl}. The greater value of n_{bp} simply allows more chance for the DSB_{cl} to be induced and in turn makes the contribution of the direct effect to the total number of DSB

appear to be smaller. Accordingly, the trend of decreasing D_{10} value with increasing n_{bp} found for both SS and SB methods is as expected.

The decreases in the ratios of SSB and BD to DSB resulting from the increase in n_{bp} are due to the fact that portions of SSB and BD were used in the formation of DSB_{cl}; the more DSB_{cl} being produced, the less SSB and BD being left intact. The quantitative results presented in this section can be useful when predicting the radiosensitivity of the cells given that additional information is available. For instance, the model can be used to evaluate the difference in the radiation resistance of the wild-type cells and the mutants that are deficient in repair of certain forms of damaged DNA. Moreover, the ability to differentiate the type of DSB can be beneficial because not every DSB poses the same level of threat to the cell survivability, e.g., blunt ends are known to be more difficult to repair than sticky ends (Moiseenko et al.,1998).

A constant value of n_{bp} is typically used by many modelers (Moiseenko et al.,1998). However, a variety of repair mechanisms performed by different enzymes in the actual cells exhibit an array of unique behaviors. Furthermore, in addition to the hydrogen bonds in the DNA double helix, other cellular molecules such as DNA binding proteins also play roles in holding the two DNA strands together. Thus, a single number of n_{bp} may not adequately represent the condition in vivo. If important factors relevant to n_{bp}, e.g., the precise frequency of each major type of DNA damage and the nature of the repair process or the absolute amount of energy needed to maintain the normal configuration of the DNA molecule, can be quantitatively identified, a specific value or distribution should be assigned to each situation instead of utilizing one particular threshold value for all cases.

Effect of the reaction radii

The probability of different kinds of interactions that produce DNA lesions is dictated by the magnitudes of the reaction radii. The differences among the reaction radii contribute to the dominance of the indirect effect observed in the results shown in the previous sections. Under diverse conditions of radiation treatment, the relation between the direct and indirect effects can vary to a great extent. To assess the effect of the changes in the reaction radius on the cell

reproductive death, the reaction radius derived from the BEB formalism, $r_{BEB-DNA}$, as well as the reaction radii for the reactions between DNA constituents and water radicals, i.e., r_{OH-DNA} and $r_{e_{aq}^- - DNA}$, were adjusted individually to different percentages of the values adapted from the literature while other parameters were kept constant.

The D_{10} values of *E. coli* O157:H7 resulting from the changes in the sizes of the reaction radii are provided in Figure 4.3. The corresponding relative contributions of the direct effect to the total DSB yields are shown in Figure 4.4. Note that the SB method with n_{bp} value of 10 was employed to determine the D_{10} values in this and the subsequent sections. The reference D_{10} value, if not mentioned otherwise, is referred to the D_{10} value of *E. coli* O157:H7 obtained originally which is 0.357 kGy.

The general trends of variation in the D_{10} values in relationship to the relative modification of the three reaction radii are as expected; the longer the reaction radius, the greater the probability of interaction with the DNA, and consequently, the more the DNA damage, the lower the D_{10} value. The relative contribution of direct ionization in terms of the production of DSB increases with increasing $r_{BEB-DNA}$ and decreases with increasing r_{OH-DNA} and $r_{e_{aq}^- - DNA}$ as can be explained by the probabilities implied by these parameters. The larger the reaction radius for the direct ionization by electrons, the greater the chance that the DSB_{di} can be formed. On the contrary, the greater the reaction radii for the reactions with water radicals, the higher the probabilities that the DSB_{cl} will be produced, and accordingly, the more the contributions of DSB_{cl} to the total numbers of DSB, the smaller the relative amounts of DSB_{di}.

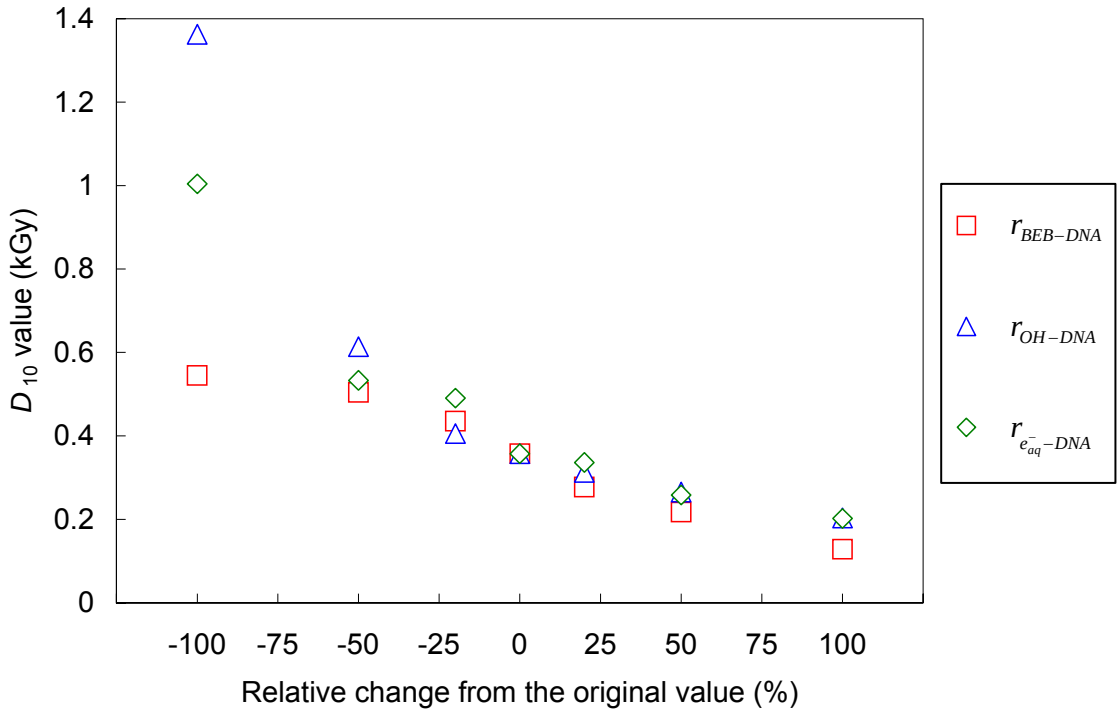

Figure 4.3. Effect of different values of the reaction radii for the interactions with DNA on the calculated D_{10} values

The ranges of both D_{10} values and percentages of DSB due to the direct effect are greatest for the case of the attack on the DNA by the OH radical, followed by DNA reaction with the e_{aq}^-, and direct DNA interaction with the ionizing particle. The relative magnitudes of these ranges conform to the predictions that could be made simply by comparing the values of the reaction radii. Nevertheless, these results indicate that when the stochastic processes in this developed model are accounted for, the relative impacts of the DNA damaging agents still remain in the same order.

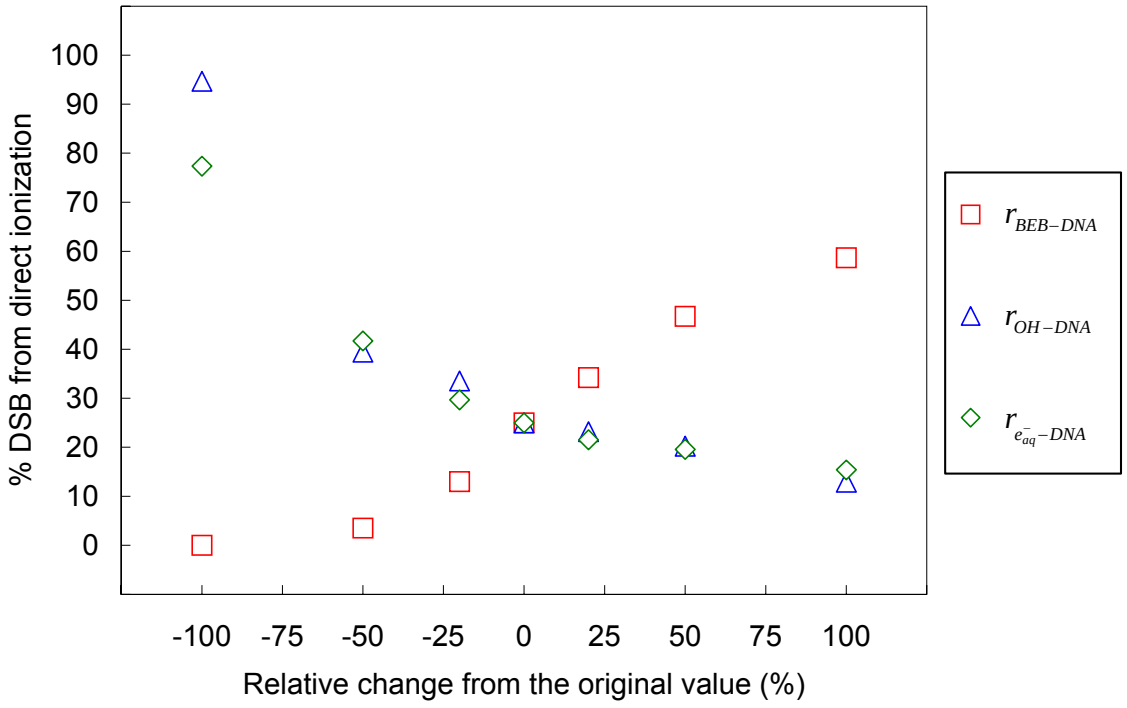

Figure 4.4. Changes in the fraction of DSB induced by direct ionization due to the variation of the reaction radii

If no interaction exists between the OH radical and the DNA molecule, the radiation resistance would be much greater; the D_{10} value becomes nearly quadruple. The effect is less pronounced in the case of the e_{aq}^- where the D_{10} value increases by almost three times. The fact that the e_{aq}^- has insignificant impact on the ribose-phosphate backbone unlike the OH is probably the underlying cause of this difference. Under the circumstance that the possibility of DNA damage from direct ionization can be completely ignored, the results show that the D_{10} value increases by about 50%.

In a special case (not shown in Figure 4.3.) where the indirect actions of ionizing radiation are strictly prohibited, i.e., every DNA lesion solely results from the direct energy absorption, the calculated D_{10} value turns out to be 1.472 kGy. This value is higher than that resulting from the situation where either the reaction of the OH or e_{aq}^- with DNA alone is excluded.

A relatively large decrease in the D_{10} value results when half the value of the reaction radius for the reaction of the OH radical with DNA as opposed to zero is employed. A smaller decrease (47% instead of 55% reduction) is observed in the case of the e_{aq}^{-}; whereas for $r_{BEB-DNA}$, a much less degree of reduction (<8% decrease) is found. When the reaction radii are varied from 50 to 200% of their original values, the D_{10} values for all three cases appear to be gradually reduced having the magnitudes comparable to each other.

The environment of the actual irradiation process is not always the same as that assumed in the model and can differ appreciably. For example, some irradiation facilities operate at room temperature, while others perform the treatment at about the freezing point; several food products are irradiated under standard atmospheric pressure, whereas certain items are previously packed in modified atmospheres. In general, the results in this section signify the relative importance of each DNA damaging agent within the range of the parameter values being studied. The information presented can be applied to the prediction of the radiation sensitivity of bacteria when they are subjected to irradiation under different conditions that could alter the efficiency of radiation in inducing DNA damage.

Effect of the scavengers

Many species besides water are present in the bacterial cells. The presence of these cellular components can significantly affect the lethality of the irradiation treatment. The effectiveness of the indirect action of radiation depends on the degree to which the radiolytic radicals produced from water radiolysis can cause the damage to DNA. Any substance that can scavenge free radicals, regardless of its origin, can potentially reduce the number of DNA lesions. The characteristic absorption time, t_{ab}, was introduced into the model to characterize the reduction of chemical species due to the scavenging effect. The results of DNA damage obtained for different values of t_{ab} are provided in Table 4.4.

Table 4.4. The percentages of DNA damage caused by direct energy deposition and the calculated D_{10} values of *E. coli* O157:H7 for different concentrations of scavengers

Characteristic absorption time (10^{-10} s)	% DSB direct	% SSB direct	% BD direct	D_{10} (kGy)*
~ 0	41.80	40.62	2.90	0.628 [a]
3	27.74	6.14	1.00	0.365 [b]
6	25.00	5.27	0.90	0.357 [b]
9	24.15	5.11	0.94	0.358 [b]
12	24.34	5.05	0.93	0.350 [b]
∞	24.87	4.68	0.87	0.353 [b]

* The D_{10} values with the same superscript letter are not significantly different ($p < 0.05$).

The D_{10} value corresponding to t_{ab} of zero is significantly higher than any D_{10} values associated with other values of t_{ab}. The D_{10} value seems to decrease with increasing t_{ab} for $0 \leq t_{ab} \leq 6\text{x}10^{-10}$ s. For the higher t_{ab}, the D_{10} values fluctuate. Similar effects are observed for the relative contributions of the direct effect to the productions of DSB, SSB, and BD. Different values of t_{ab} represent different capacities of scavengers; the smaller the t_{ab}, the greater the scavenging capability. The larger the t_{ab}, the longer the time in which chemical species are free for interaction. The probabilities that reactive water radicals could react with DNA increase with t_{ab}. In contrast, the direct-type DNA damage is independent of t_{ab}. The general trend of decreasing percentages of DNA damage from direct energy deposition is caused by the increasing amounts of DNA lesions due to the indirect effect.

In the case that t_{ab} is indefinitely small, every radiolytic species is absorbed immediately before they could begin to diffuse. However, if water radicals are formed in a close enough proximity with DNA constituents, the reactions will take place. The comparison between the result in this case and that calculated when the indirect action of radiation is prohibited (the reaction radii for water radicals-DNA are set to zero) shows that much of the damage by radical attacks occurs within the first few picoseconds. The relative contribution of direct ionization to the total number of DSB drops from 100 to 41.80% and the D_{10} value decreases from 1.472 to 0.628 kGy when the radicals are able to interact with the DNA but not diffuse as opposed to the complete absence of radical mediated pathways.

In the opposite situation where radiolytic radicals can freely diffuse and interact with DNA and water radiolysis products without interference from any other cellular substance, the killing effect of irradiation is not significantly different from that under normal cellular conditions. The equality between the two D_{10} values indicates that the condition of the bacterial cell is basically the same as that of the pure water in spite of the incorporation of t_{ab} in the model. Though other aspects of DNA damage corresponding to t_{ab} of infinity are as expected, i.e., different percentages of DNA lesions due to the direct effect are essentially the lowest because of the relative quantities of radical-induced DNA damage, the increased amounts of the indirect-type lesions are not sufficient to produce a significantly lower D_{10} value. This observation suggests that the effectiveness of the current use of t_{ab} might be questionable. The fact that once the species diffuse out of the detector, potential reactions for those species are discarded could contribute to the underestimation of DNA damage from reactions with active radical species.

The external factors such as food medium and environmental condition capable of altering the chemical composition of the cells can be directly related to the scavenging capacity. t_{ab} utilized in the model can be adjusted to accommodate the changes inside the cell caused by these factors. However, employing one value of t_{ab} to characterize the nature of the interactions between the radicals and the cellular components may lead to oversimplification of the decay of various chemical species. Many biological molecules have different specificities for certain substrates. Instead of using a universal number, the use of individual t_{ab} unique for each radiolytic species could be a better alternative.

Effect of the detector size

The size of the detector was deduced from the morphological characteristic of *E. coli* by assuming that DNA is uniformly dispersed in the nucleoid region of the cell. The dimensions of the cell and the nucleoid do not change in the calculation. For simplicity, only one DNA double helix is present inside the detector. Thus far, the calculations in the previous sections were based on the detector volume of 343 nm^3, i.e., the length of each side of the detector box is 7 nm. By varying the size of the detector, the amount of DNA lesions from both direct and indirect

mechanisms of radiation damage would be altered. The calculated D_{10} values as well as the relative changes in the quantities of DNA damage for different detector volumes are presented in Table 4.5. The percent changes in the DNA lesions are the relative changes in the amount of damage per the same unit of volume and radiation dose resulted from the modification of the detector size from the original design.

Table 4.5. The percentages of change in the DNA damage due to the variation in the detector size and the calculated D_{10} values of *E. coli* O157:H7 for different detector volumes

Detector volume (nm^3)	% Δ in volume from the base model	% Δ in DNA lesion			D_{10} (kGy)
		DSB	SSB	BD	
125	-63.6	258.14	146.97	140.88	0.092
216	-37.0	42.90	22.32	22.74	0.247
343	0.0	0.00	0.00	0.00	0.357
512	49.3	-55.37	-55.06	-54.31	0.814
1000	191.5	-65.61	-60.59	-61.05	1.059
1728	403.8	-76.64	-67.22	-70.62	1.564

In general, the larger the size of the detector that contains a single DNA molecule, the less the chance that the damaging agents will be located near one of the DNA constituents or reach it at the later time. At the same level of radiation dose, the average number of lesions per unit volume would be smaller for larger detector size regardless of the type of DNA lesion. The calculations show that the effects of the detector size on the relative changes in the productions of SSB and BD are comparable. The reduction in the detector volume affects the induction of DSB the most. The impact on the amount of DSB can also be observed from the increase in the calculated D_{10} value with the increasing detector volume.

As mentioned earlier, DSB can be produced either by the energy deposition or the conversion of elementary damages (SSB and BD). The latter mechanism of DSB formation consumes fractions of SSB and BD, and therefore, its capacity depends on the quantities of those lesions. While the production of DSB_{cl} increases, larger quantities of SSB and BD are being used. The relationship between the formation of DSB and the consumption of BD and SSB could explain the observation that the detector size has the greatest impact on the percent change in the number of DSB.

In this proposed model, all parameters regarding the geometry of the cells are treated as constant, which is in contrast to the real situation where the geometric properties of the cells change throughout the cell cycle (Kim, Yoshimura, Hizume, Ohniwa, Ishihama & Takeyasu, 2004; Nanninga & Woldringh, 1985). Many extrinsic and intrinsic factors such as temperature, pressure, and medium composition can affect the morphological characteristics of the cell. Any major factor that could lead to the change in cell morphology should be considered when designing the detector. Since the modification of the detector size can greatly influence the amount of DNA damage, using the distribution of geometrical parameters in the model could significantly improve the computational algorithm.

Effect of G_{eq}

The quantity of genetic material in the nucleoid region does not usually equal to that of one complete genome of the bacterium nor does it remain unchanged over an extended period of time under normal metabolic conditions. The parameter G_{eq} was introduced so that the impact of variation in the amount of genome can be assessed. This parameter was employed in the calculation after DNA damage was determined; thereby G_{eq} has no influence on the detailed results of DNA lesions. However, G_{eq} was used in the construction of survival curves from which the D_{10} values were determined. The effect of G_{eq} on the radiation sensitivity of *E. coli* O157:H7 is depicted in Figure 4.5.

When G_{eq} is greater than 1, the shoulder on the curve of survival probability appears. The result implies that more radiation might be required at low doses to inhibit cell proliferation. In order for the cell to become reproductively dead, at least one DSB must occur in each complete genome. The survival curves associated with different values of G_{eq} show that the D_{10} values, which were calculated from the linear portions of the semi-log plots, do not change with G_{eq}. When the entire population has been exposed to a high enough amount of radiation, the probability that an active cell will become clonogenically dead by an increment of radiation dose is equivalent to the probability of induction of a DSB when only one complete genomic sequence is present in the cell.

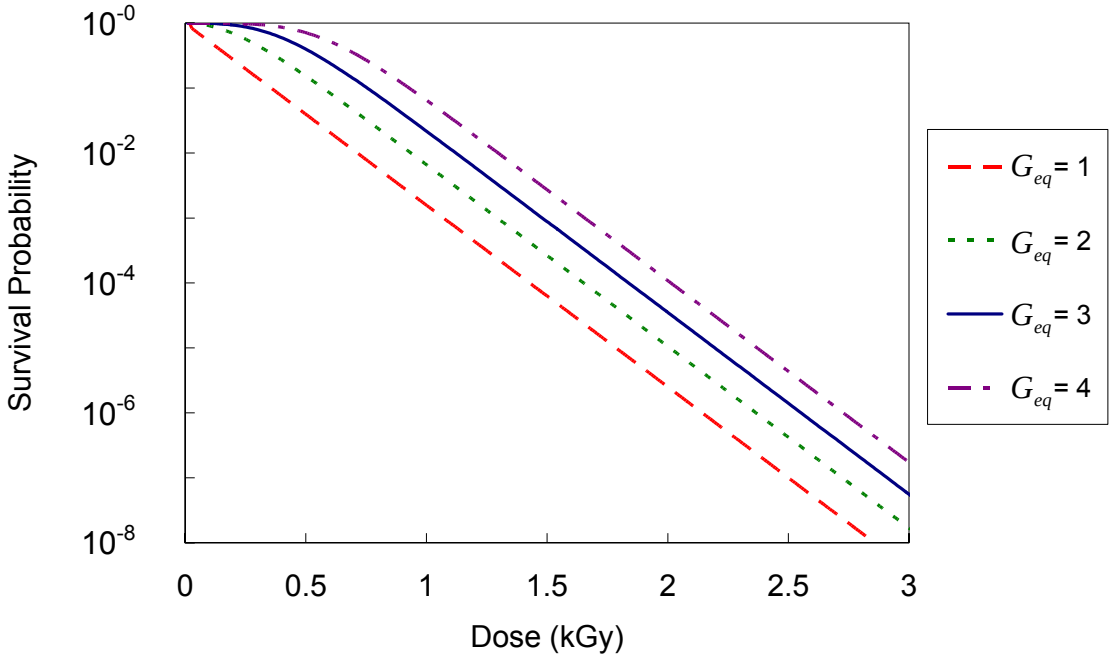

Figure 4.5. Survival curves of *E. coli* O157:H7 with different G_{eq}

The parity of the D_{10} values for different G_{eq} indicates that if the radiation sensitivity of the cells is expressed in terms of D_{10} values, additional DNA beyond the size of the genome does not enhance the radiation resistance. On the contrary, if the D_{10} values were to be determined by using the entire survival curves, which include the coordinates of the origins, the D_{10} values would be greater for higher G_{eq}. For this reason, the use of D_{10} value to characterize the radiation sensitivity of a microorganism might not be sufficient especially at low dose levels even if the kinetics of repair processes of the microbe can be proven to be of the first order.

In a regular food item at its natural state, typically, there is a mixture of cells at different phases of growth at any given moment. The mass of DNA contained in the cell varies as the cell progresses through the cell cycle (Nanninga & Woldringh, 1985). Relevant information such as the nutrients in the medium and the temperature during the storage prior to radiation processing that can greatly influence the amount of DNA inside the nucleoid could be employed to generate a distribution of G_{eq} for the calculation of the lethal probability. However, if the model is to be used

to design the radiation treatment, from the food safety standpoint, at least the highest value of genome equivalent found in the entire microbial population must be utilized in the algorithm to ensure that the most resistant ones have been inactivated.

Review of the proposed model and suggestions for improvement

The developed model can be used to examine the radiation effects on the target organism by simulating the processes of interaction in the cells. Because the model can assess the damage caused by radiation at the DNA level, several implications can be drawn from the details of the resulting DNA lesions. At this stage of the model development, the proposed algorithm cannot yet universally predict the D_{10} values of specific microorganisms in particular food commodities. Nevertheless, this model can be employed as an investigative tool in complement with other available methods to gain better understanding of the impact of radiation exposure.

Certainly, many trends of the increase and decrease in different forms of the results representing DNA damage in relation to the variation of the selected parameters discussed above can arguably be speculated without rigorous calculations performed by the model. However, the actual amount of impact cannot be easily estimated due to the stochastic nature of the process and complication arose from interrelations among different factors. The numerical results obtained from this model at the current stage are not to be regarded as absolute numbers. These quantitative results should be used for qualitative analysis.

Several mathematical formalisms and parameters were utilized to construct the model. In turn, it can be divided into distinct parts. Each contributes to both the accuracy and uncertainty of the final result and can be potentially adjusted or improved either separately or in combination with related components. Some parts of the model such as the diffusion mediated reactions in the chemical stage have been extensively employed for this type of calculation in the literature, others like the use of $r_{BEB-DNA}$ derived from the electron impact ionization cross section have never been proposed before. More benefits provided by a model like the one developed in

this research can be gained by dissection of the algorithm rather than interpretation of the results alone. The research areas that should be further investigated in future studies are listed below:

- Energy deposition of electrons in the cells of microorganisms

There are a number of simulation toolkits for particle transport that can be utilized to generate the track structure beside GEANT4. Many of which developed by different researchers employ the same database of cross sections. However, there are differences in the choice of theoretical models and how the experimental data is incorporated into these codes (Nikjoo et al., 2006). Systematic comparison of the track structures obtained from different codes and the D_{10} values calculated by coupling the resulting detailed energy deposition with other parts of the algorithm in the proposed model can be made to evaluate the discrepancy in the results. Dependency on certain input parameters other than the ones investigated in this study such as the primary electron energy can also be examined.

Modification of the model should be performed to take into account the dissimilarity between the physical properties of pure liquid water and materials that compose the cell. For instance, the mass collision stopping powers of the materials that are similar to water can be estimated using the average ratios of the atomic number to the mass number, the excitation energies, the densities, the coefficient of variation of collision stopping power with respect to the mean excitation energy, and the corresponding coefficient of variation with respect to density (ICRU, 1984). The significance of the differences between the parameters of the pure liquid water and the cells could be more prominent in the microscopic scale.

- Design of DNA molecules in the bacterial cell with the presence of other cellular components

The organization of the DNA in the bacterial nucleoid is influenced by the physical condition, e.g., the concentration of different macromolecules, the degree of supercoiling, etc., as well as the physiological condition of the metabolic process in which the DNA is being involved (Woldringh & Odijk, 1999). In the proposed model, there is only one straight B-form DNA duplex

contained inside each detector without physical contact to any other cellular substance. Interference due to the presence of diverse compounds in the living cells is inevitable. For example, the accessibility of the active water radicals to the DNA molecules would be reduced by the attached nucleoid components such as DNA binding proteins. However, these components could provide additional sources of secondary electrons close to the DNA (Bernhardt et al., 2002). The changes in DNA geometry in the dynamic cellular environment and when other nucleoidal materials are introduced along with the protective and detrimental effects attributed to these associated biomolecules could significantly affect the calculated D_{10} values.

- Cross sections for the electron impact ionization of DNA and the basis set input

The ionization cross sections used to derive the reaction radii for direct ionization of the DNA constituents were determined from the BEB formalism employing the scaled binding energy and the average orbital kinetic energy of the target electron from the RHF/3-21G basis set. The calculated BEB cross sections of various molecules and free radicals were reported to generally agree well with those from other theoretical calculations and experimental data (Deutsch, Becker, Matt & Mark, 2000). Nevertheless, different formalisms with the more sophisticated quantum mechanical parameters can be implemented in the developed model for result comparison. More importantly, the method for the derivation of $r_{BEB-DNA}$ should be analytically validated. The results of the relative contributions of the direct and indirect effects can only be reliable if the assumption made is reasonably accurate.

- Ionization and excitation of liquid water and related biomolecules

At the moment, the cross sections for liquid water have been derived from the fusion of data for water in both the liquid and vapor phases. The direct empirical data for excitation and ionization cross sections of liquid water are not available because of the difficulty of experimental measurement and the limited knowledge of electron interactions with liquid water (Itikawa & Mason, 2005; Nikjoo et al., 2006). Future experiments to determine the cross sections as well as the study of ionization and excitation dissociation schemes for the interaction of electrons in liquid

water could provide more accurate estimates for model inputs. In addition, the cross sections for electron interactions with other cellular molecules relevant to the induction of DNA damage can also be utilized in the proposed model.

- Chemical reactions inside the cells due to the food intake and environmental factors

The nutrients in the food medium definitely play an important role in the overall functionality of the residing microorganisms. The radiation resistance of the same strain of microbe growing in diverse food samples can be different. Moreover, the evidence that several additives can be used to manipulate the radiosensitivity of bacteria (Ahn et al., 2006; Borsa et al., 2004) confirms that responses to radiation are highly dependent on the food environment. One of the ways that the impact of food composition and other modifiers can be accounted for is to include additional chemical reactions in the algorithm. Furthermore, the amount of species available for reaction, which is regulated by the environmental condition, should be taken into consideration as well.

Final note

There are other significant factors that were not discussed in this study such as the microorganism's ability to adapt and develop greater resistance to radiation stress (Levanduski & Jaczynski, 2008) and the probability of mutations that could considerably affect the bacterial radiation sensitivity. Unquestionably, the quest to thoroughly understand the living organisms to the point that accurate predictions of the biological responses can be made is a difficult task. More research is still required before sufficient knowledge can be attained.

CHAPTER V

CONCLUSIONS

A theoretical model for the calculation of the D_{10}-value has been developed. Both direct and indirect effects of irradiation on bacterial DNA were assessed through the simulation of radiation damage utilizing the step-by-step Monte-Carlo method. The sensitivity analysis was performed on several variables to investigate the efficiency of radiation under different hypothetical scenarios. The results obtained are generally reasonable. However, the model still needs to be improved before it can be used to accurately predict the radiation response of bacteria for the design of a food irradiation treatment. Nevertheless, the proposed computational algorithm provides a means to mechanistically study the action of radiation at the molecular level. The presented methodology can be employed as an analytical technique complementary to other approaches to understand the physical, chemical, and biological changes in the cells exposed to energetic electrons.

REFERENCES

Agostinelli, S., Allison, J., Amako, K., Apostolakis, J., Araujo, H., Arce, P., et al. (2003). GEANT4-a simulation toolkit. *Nuclear Instruments & Methods in Physics Research Section a-Accelerators Spectrometers Detectors and Associated Equipment*, *506*(3), 250-303.

Ahn, D. U., Lee, E. J., & Mendonca, A. (2006). Meat decontamination by irradiation. In L. M. L. Nollet, & F. Toldrá (Eds.), *Advanced technologies for meat processing* (pp. 155-191). Boca Raton, FL: CRC/Taylor & Francis.

Alpen, E. L. (1998). *Radiation biophysics*. San Diego, CA: Academic Press.

Amako, K., Guatelli, S., Ivanchenko, V. N., Maire, M., Mascialino, B., Murakami, K., et al. (2005). Comparison of GEANT4 electromagnetic physics models against the NIST reference data. *IEEE Transactions on Nuclear Science*, *52*(4), 910-918.

Attix, F. H. (1986). *Introduction to radiological physics and radiation dosimetry*. New York: Wiley.

Aydogan, B., Bolch, W. E., Swarts, S. G., Turner, J. E., & Marshall, D. T. (2008). Monte Carlo simulations of site-specific radical attack to DNA bases. *Radiation Research*, *169*(2), 223-231.

Ballarini, F., Biaggi, M., Merzagora, M., Ottolenghi, A., Dingfelder, M., Friedland, W., et al. (2000). Stochastic aspects and uncertainties in the prechemical and chemical stages of electron tracks in liquid water: a quantitative analysis based on Monte Carlo simulations. *Radiation and Environmental Biophysics*, *39*(3), 179-188.

Bernhardt, P., Friedland, W., Meckbach, R., Jacob, P., & Paretzke, H. G. (2002). Monte Carlo simulation of DNA damage by low LET radiation using inhomogeneous higher order DNA targets. *Radiation Protection Dosimetry*, *99*(1-4), 203-206.

Bernhardt, P., & Paretzke, H. G. (2003). Calculation of electron impact ionization cross sections of DNA using the Deutsch-Mark and Binary-Encounter-Bethe formalisms. *International Journal of Mass Spectrometry*, *223*(1-3), 599-611.

Borsa, J., Lacroix, M., Ouattara, B., & Chiasson, F. (2004). Radiosensitization: Enhancing the radiation inactivation of foodborne bacteria. *Radiation Physics and Chemistry*, *71*(1-2), 137-141.

Busta, F. F., Peterson, E. H., Adams, D. M., & Johnson, M. G. (1984). Colony count methods. In M. L. Speck (Ed.), *Compendium of methods for the microbiological examination of foods* (pp. 62-83). Washington, DC: American Public Health Association.

Chadwick, K. H., & Leenhouts, H. P., (1973). A molecular theory of cell survival. *Physics in Medicine and Biology*, *18*(1), 78-87.

Chang, P. W., Zhang, Q. M., Takatori, K., Tachibana, A., & Yonei, S. (2005). Increased sensitivity to sparsely ionizing radiation due to excessive base excision in clustered DNA damage sites in *Escherichia coli*. *International Journal of Radiation Biology*, *81*(2), 115-123.

Chatterjee, A., & Holley, W. R. (1991). Energy deposition mechanisms and biochemical aspects of DNA strand breaks by ionizing-radiation. *International Journal of Quantum Chemistry*, *39*(5), 709-727.

Crawford, L. M., & Ruff, E. H. (1996). A review of the safety of cold pasteurization through irradiation. *Food Control*, *7*(2), 87-97.

Curtis, S. B. (1986). Lethal and potentially lethal lesions induced by radiation - a unified repair model. *Radiation Research*, *106*(2), 252-270.

Deutsch, H., Becker, K., Matt, S., & Mark, T. D. (2000). Theoretical determination of absolute electron-impact ionization cross sections of molecules. *International Journal of Mass Spectrometry*, *197*, 37-69.

GEANT4 Collaboration (2007). *GEANT4 physics reference manual.* <http://geant4.web.cern.ch/geant4/>

Goodhead, D. T. (2006). Energy deposition stochastics and track structure: What about the target? *Radiation Protection Dosimetry*, *122*(1-4), 3-15.

Green, A. E. S. (1975). Role of secondary electrons in charged-particle degradation. *Radiation Research*, *64*(1), 119-140.

Hamm, R. N., Turner, J. E., & Stabin, M. G. (1998). Monte Carlo simulation of diffusion and reaction in water radiolysis - a study of reactant 'jump through' and jump distances. *Radiation and Environmental Biophysics*, *36*(4), 229-234.

Hill, M. A., & Smith, F. A. (1994). Calculation of initial and primary yields in the radiolysis of water. *Radiation Physics and Chemistry*, *43*(3), 265-280.

Hoeijmakers, J. H. J. (1993). Nucleotide excision repair 1: from *E. coli* to yeast. *Trends in Genetics*, *9*(5), 173-177.

IAEA (International Atomic Energy Agency) (2002). *Dosimetry in food irradiation*. Vienna, AT: International Atomic Energy Agency.

ICMSF (International Commission on Microbiological Specifications for Foods) (1996). *Microorganisms in foods 5 : Characteristics of microbial pathogens*. London: Blackie Academic & Professional.

ICRU (International Commission on Radiation Units and Measurements) (1984). *Stopping powers for electrons and positrons*. Bethesda, MD: International Commission on Radiation Units and Measurements.

Itikawa, Y., & Mason, N. (2005). Cross sections for electron collisions with water molecules. *Journal of Physical and Chemical Reference Data*, *34*(1), 1-22.

Kellerer, A. M., & Rossi, H. H. (1978). Generalized formulation of dual radiation action. *Radiation Research*, *75*(3), 471-488.

Kim, J., Moreira, R. G., Huang, Y., & Castell-Perez, M. E. (2007). 3-D dose distributions for optimum radiation treatment planning of complex foods. *Journal of Food Engineering*, *79*(1), 312-321.

Kim, J., Moreira, R. G., Rivadeneira, R., & Castell-Perez, M. E. (2006). Monte Carlo-based food irradiation simulator. *Journal of Food Process Engineering*, *29*(1), 72-88.

Kim, J., Rivadeneira, R. G., Castell-Perez, M. E., & Moreira, R. G. (2006). Development and validation of a methodology for dose calculation in electron beam irradiation of complex-shaped foods. *Journal of Food Engineering*, *74*(3), 359-369.

Kim, J., Yoshimura, S. H., Hizume, K., Ohniwa, R. L., Ishihama, A., & Takeyasu, K. (2004). Fundamental structural units of the *Escherichia coli* nucleoid revealed by atomic force microscopy. *Nucleic Acids Research*, *32*(6), 1982-1992.

Kim, Y. K., Hwang, W., Weinberger, N. M., Ali, M. A., & Rudd, M. E. (1997). Electron-impact ionization cross sections of atmospheric molecules. *Journal of Chemical Physics*, *106*(3), 1026-1033.

Kow, Y. W. (1994). Base excision repair in *E. coli* - an overview. *Annals of the New York Academy of Sciences*, *726*, 178-180.

Kutcher, G. J., & Green, A. E. S. (1976). Model for energy deposition in liquid water. *Radiation Research*, *67*(3), 408-425.

Laverne, J. A., & Mozumder, A. (1993). Concerning plasmon excitation in liquid water. *Radiation Research*, *133*(3), 282-288.

Lea, D. E. (1955). *Actions of radiations on living cells*. Cambridge, UK: University Press.

Levanduski, L., & Jaczynski, J. (2008). Increased resistance of *Escherichia coli* O157:H7 to electron beam following repetitive irradiation at sub-lethal doses. *International Journal of Food Microbiology*, *121*(3), 328-334.

Lodish, H., Berk, A., Zipursky, S. L., Matsudaira, P., Baltimore, D., & Darnell, J. (2000). *Molecular cell biology*. New York: W.H. Freeman.

Moiseenko, V. V., Hamm, R. N., Waker, A. J., & Prestwich, W. V. (1998). Modelling DNA damage induced by different energy photons and tritium beta-particles. *International Journal of Radiation Biology*, *74*(5), 533-550.

Monk, J. D., Beuchat, L. R., & Doyle, M. P. (1995). Irradiation inactivation of food-borne microorganisms. *Journal of Food Protection*, *58*(2), 197-208.

Muroya, Y., Meesungnoen, J., Jay-Gerin, J. P., Filali-Mouhim, A., Goulet, T., Katsumura, Y., & Mankhetkorn, S. (2002). Radiolysis of liquid water: An attempt to reconcile Monte-Carlo calculations with new experimental hydrated electron yield data at early times. *Canadian Journal of Chemistry-Revue Canadienne De Chimie*, *80*(10), 1367-1374.

Nanninga, N., & Woldringh, C. L. (1985). Cell growth, genome duplication, and cell division. In N. Nanninga (Ed.), *Molecular cytology of* Escherichia coli (pp. 259-318). London: Academic Press.

Nelson, D. L., & Cox, M. M. (2005). *Lehninger principles of biochemistry*. New York: W.H. Freeman.

Nelson, K. E., Fouts, D. E., Mongodin, E. F., Ravel, J., DeBoy, R. T., Kolonay, J. F., et al. (2004). Whole genome comparisons of serotype 4b and 1/2a strains of the food-borne pathogen *Listeria monocytogenes* reveal new insights into the core genome components of this species. *Nucleic Acids Research*, *32*(8), 2386-2395.

Niemira, B. A. (2003). Irradiation of fresh and minimally processed fruits, vegetables, and juices. In J. S. Novak, G. M. Sapers, & V. K. Juneja (Eds.), *Microbial safety of minimally processed foods* (pp. 279-299). Boca Raton, FL: CRC Press.

Nikjoo, H., Bolton, C. E., Watanabe, R., Terrissol, M., O'Neill, P., & Goodhead, D. T. (2002). Modelling of DNA damage induced by energetic electrons (100 eV to 100 keV). *Radiation Protection Dosimetry*, *99*(1-4), 77-80.

Nikjoo, H., O'Neill, P., Goodhead, D. T., & Terrissol, M. (1997). Computational modelling of low-energy electron-induced DNA damage by early physical and chemical events. *International Journal of Radiation Biology*, *71*(5), 467-483.

Nikjoo, H., O'Neill, P., Terrissol, M., & Goodhead, D. T. (1999). Quantitative modelling of DNA damage using Monte Carlo track structure method. *Radiation and Environmental Biophysics*, *38*(1), 31-38.

Nikjoo, H., Uehara, S., Emfietzoglou, D., & Cucinotta, F. A. (2006). Track-structure codes in radiation research. *Radiation Measurements*, *41*(9-10), 1052-1074.

Olivero, J. J., Stagat, R. W., & Green, A. E. S. (1972). Electron deposition in water vapor, with atmospheric applications. *Journal of Geophysical Research*, *77*(25), 4797-4811.

Parnes, R. B., & Lichtenstein, A. H. (2004). Food irradiation: A safe and useful technology. *Nutrition in Clinical Care*, *7*(4), 149-155.

Perna, N. T., Plunkett III, G., Burland, V., Mau, B., Glasner, J. D., Rose, D. J., et al. (2001). Genome sequence of enterohaemorrhagic *Escherichia coli* O157:H7. *Nature*, *409*(6819), 529-533.

Rasmussen, L. J., Samson, L., & Marinus, M. G. (1998). Dam-directed DNA mismatch repair. In J. A. Nickoloff, & M. F. Hoekstra (Eds.), *DNA damage and repair: DNA repair in prokaryotes and lower eukaryotes* (pp. 205-228). Totowa, NJ: Humana Press.

Rodriguez, O., Castell-Perez, M. E., Ekpanyaskun, N., Moreira, R. G., & Castillo, A. (2006). Surrogates for validation of electron beam irradiation of foods. *International Journal of Food Microbiology*, *110*(2), 117-122.

Rossi, H. H., & Zaider, M. (1996). *Microdosimetry and its applications*. New York: Springer.

Rupp, W. D. (1996). DNA repair mechanisms. In F. C. Neidhardt (Ed.), Escherichia coli *and* Salmonella *: Cellular and molecular biology* (pp. 2277-2294). Washington, DC: ASM Press.

Sancar, A. (1994). Structure and function of DNA photolyase. *Biochemistry*, *33*(1), 2-9.

Shea, K. M., and the Committee on Environmental Health (2000). Technical report: Irradiation of food. *Pediatrics*, *106*(6), 1505-1510.

Sommers, C. H. (2003). Irradiation of minimally processed meats. In J. S. Novak, G. M. Sapers, & V. K. Juneja (Eds.), *Microbial safety of minimally processed foods* (pp. 301-318). Boca Raton, FL: CRC Press.

Tabata, T., Andreo, P., & Ito, R. (1991). Analytic fits to Monte-Carlo calculated depth dose curves of 1-MeV to 50-MeV electrons in water. *Nuclear Instruments & Methods in Physics Research Section B-Beam Interactions with Materials and Atoms*, *58*(2), 205-210.

Tobias, C. A. (1985). The repair misrepair model in radiobiology - comparison to other models. *Radiation Research*, *104*(2), S77-S95.

Tomita, H., Kai, M., Kusama, T., & Ito, A. (1997). Monte Carlo simulation of physicochemical processes of liquid water radiolysis - the effects of dissolved oxygen and OH scavenger. *Radiation and Environmental Biophysics*, *36*(2), 105-116.

Turner, J. E. (2007). *Atoms, radiation, and radiation protection*. Weinheim, DE: Wiley-VCH.

Uehara, S., & Nikjoo, H. (2006). Monte Carlo simulation of water radiolysis for low-energy charged particles. *Journal of Radiation Research*, *47*(1), 69-81.

Uehara, S., Nikjoo, H., & Goodhead, D. T. (1999). Comparison and assessment of electron cross sections for Monte Carlo track structure codes. *Radiation Research*, *152*(2), 202-213.

WHO (1999). High-dose irradiation: Wholesomeness of food irradiated with doses above 10 kGy. Report of a Joint FAO/IAEA/WHO Study Group. *World Health Organization Technical Report Series 890*, 1-197.

Wilkinson, V. M., & Gould, G. W. (1996). *Food irradiation : A reference guide*. Oxford, UK: Butterworth-Heinemann.

Wilson III, D. M., Engelward, B. P., & Samson, L. (1998). Prokaryotic base excision repair. In J. A. Nickoloff, & M. F. Hoekstra (Eds.), *DNA damage and repair: DNA repair in prokaryotes and lower eukaryotes* (pp. 29-64). Totowa, NJ: Humana Press.

Woldringh, C. L., & Nanninga, N. (1985). Structure of nucleoid and cytoplasm in the intact cell. In N. Nanninga (Ed.), *Molecular cytology of* Escherichia coli (pp. 161-197). London: Academic Press.

Woldringh, C. L., & Odijk, T. (1999). Structure of DNA within the bacterial cell: Physics and physiology. In R. L. Charlebois (Ed.), *Organization of the prokaryotic genome* (pp. 171-187). Washington, DC: ASM Press.

Zimmerman, J. M., & Battista, J. R. (2006). Measuring survival in microbial populations following exposure to ionizing radiation. In F. A. Rainey, & A. Oren (Eds.), *Extremophiles* (pp. 745-754). London: Academic Press.

VITA

Name: Nont Ekpanyaskun

Address: Biological and Agricultural Engineering Department

Texas A&M University, College Station, TX 77843-2117

Email Address: nont@tamu.edu

Education: B.S., Chemical Engineering, University of Wisconsin at Madison, 2002

Ph.D., Biological and Agricultural Engineering, Texas A&M University, 2009